ACS MATERIALS Au
AN OPEN ACCESS JOURNAL OF THE AMERICAN CHEMICAL SOCIETY

pubs.acs.org/materialsau

Review

Recent Development of Atmospheric Water Harvesting Materials: A Review

An Feng, Nawshad Akther, Xiaofei Duan, Shuhua Peng, Casey Onggowarsito, Shudi Mao, Qiang Fu,* and Spas D. Kolev

Cite This: https://doi.org/10.1021/acsmaterialsau.2c00027

Read Online

ACCESS | Metrics & More | Article Recommendations

ABSTRACT: The lack of freshwater has been threatening many people who are living in Africa, the Middle East, and Oceania, while the discovery of freshwater harvesting technology is considered a promising solution. Recent advances in structured surface materials, metal−organic frameworks, hygroscopic inorganic compounds (and derivative materials), and functional hydrogels have demonstrated their potential as platform technologies for atmospheric water (i.e., supersaturated fog and unsaturated water) harvesting due to their cheap price, zero second energy requirement, high water capture capacity, and easy installation and operation compared with traditional water harvesting methods, such as long-distance water transportation, seawater desalination, and electrical dew collection devices in rural areas or individual-scale emergent usage. In this contribution, we highlight recent developments in functional materials for "passive" atmospheric water harvesting application, focusing on the structure−property relationship (SPR) to illustrate the transport mechanism of water capture and release. We also discuss technical challenges in the practical applications of the water harvesting materials, including low adaptability in a harsh environment, low capacity under low humidity, self-desorption, and insufficient solar-thermal conversion. Finally, we provide insightful perspectives on the design and fabrication of atmospheric water harvesting materials.

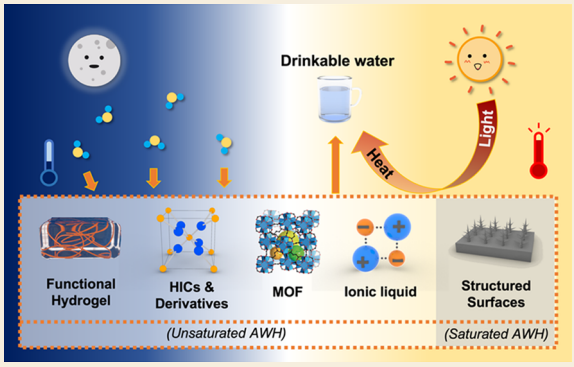

KEYWORDS: *Atmospheric water harvesting, Water crisis, Structured surface, Metal organic framework, Hygroscopic salt, Hydrogel, Ionic liquid*

1. INTRODUCTION

Water is the basis for the existence and continuation of all life on Earth. For the human body, it not only is essential for maintaining the electrolyte balance but also is the only carrier for the excretion of unwanted metabolites from the human body. The water resources on Earth are extremely abundant (ca. 1.46×10^{16} cubic meters). However, 99.97% of the water exists in the form of seawater or deep groundwater that is difficult to collect, and only less than 0.03% can be easily used by humans.[1−3] This part of our water resources mainly includes surface freshwater, water vapor in the air, and shallow groundwater. Today, due to geographical and climate constraints, the shortage of freshwater is of concern to 2.8 billion people in 48 countries all over the world especially in Africa, the Middle East, and Oceania, and the affected population may rise to 4 billion based on reasonable predictions.[4,5] Consequently, the discovery of next-generation freshwater harvesting technologies with low-cost, high-water adsorption capacity, and ease of installation and use is considered a promising solution to this global challenge and has attracted increasing attention all over the world.

There are three forms of water existing in the air: solid (i.e., snow, hail, frost, ice crystals etc.), liquid (i.e., rain, dew and fog), and gaseous (i.e., vapor, steam etc.). Humans have a long history of directly utilizing solid and liquid water, yet the capture of gaseous water has been overlooked. Currently, due to the geographical and technological limitations and climate changes, water conservancy approaches in deserts or wastelands, including energy required "active" dew collection (e.g., electricity driven condenser), liquid water transfer facilities (i.e., river diversion, long-distance water transportation, dam and reservoir construction), and seawater desalination systems usually require high investments,[6,7] high maintenance costs[8] and/or high operating costs,[9,10] high environmental impacts, inflexible installation (fixed location), and time-consuming and

Received: March 18, 2022
Revised: May 17, 2022
Accepted: May 19, 2022

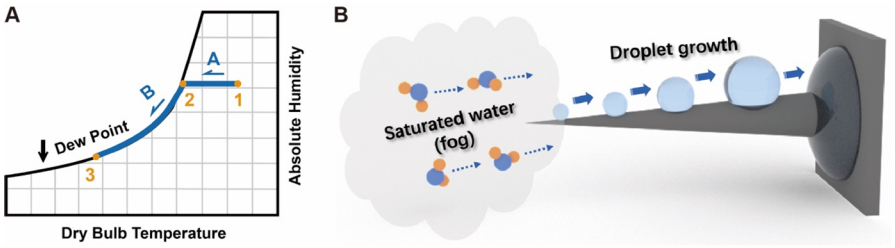

Figure 1. (A) Psychrometric chart for air−water system and water condensation mechanism. (B) Schematic illustration of dew water growth and transportation on biomimic conical spine.

seasonal intermittent water supply issues.[11,12] In recent years, "passive" water production technologies have attracted considerable attention because they do not consume second energy. For instance, researchers have developed various solar vapor generators (SVGs) composed of hydrophilic matrix and photothermal materials.[13,14] The SVG devices can float on the sea/water surface and utilize solar energy to produce clean water. Likewise, "passive" technologies for directly atmospheric water harvesting using synthetic materials are considered as promising alternatives to conventional methods due to their low cost, low energy consumption, ease of installation, and high harvesting performance when rapid water harvesting is required or electricity support is insufficient.[15] Recently, chemically designed atmospheric water harvesting (AWH) materials, including structured surface materials, metal−organic frameworks (MOFs), hygroscopic inorganic compounds and derivatives (HICs and derivatives), and functional hydrogels have attracted increasing attention. Different from the traditional water harvesting methods such as reverse osmosis desalination which uses secondary energy (e.g., electricity) or phase change condensation using cold fluids, the water harvesting mechanism of chemically designed AWH materials is based on their physical and chemical properties, including Laplace pressure gradients, chemical modifications of polymer chains, tunable intermolecular space, and open metal sites.

In this Review, we focus on the research output of passive technologies for atmospheric (gaseous) water harvesting in the past decade and provide comprehensive discussion on the state-of-the-art materials from the perspective of materials chemistry. According to the degree of water saturation, these materials are divided into two categories: (a) structured surface used for saturated atmospheric water collection and (b) MOFs, HICs and derivatives, ionic liquids (ILs), and functional hydrogels used for unsaturated vapor capture and water production. At the end of the discussion mentioned above, future perspectives and potential optimization approaches are presented which can further improve the water production performance so that it can meet energy sustainability and carbon neutral economy requirements.

2. SATURATED WATER HARVESTING

Saturated water consists of tiny water droplets evenly dispersed in the air under a supersaturated state. Figure 1 presents the psychrometric chart for a gas−water mixture and saturated water collection mechanism. The collection of unsaturated water is carried out in two steps (Figure 1A). First, water vapor is adsorbed on the surface of the hydrophilic AWH material. A drop in temperature to the dew point temperature will induce the humidity to increase to 100% (saturated state, point 1 to point 2), and then the water molecules are liquefied and stored in the AWH materials. On the other hand, the fog harvesting refers to the continuous accumulation of supersaturated small water droplets (fog) to form large water droplets, which are eventually collected on cold structural surfaces. In the past decade, this phenomenon has been observed in dense metal networks and spider webs and a variety of network materials with different structures, shapes, angles, and mesh densities for saturated water harvesting have been developed.[16,17] Notably, various saturated water harvesting systems that consume electricity to condense water have been developed and reviewed elsewhere, however this review will focus on spontaneous saturated water harvesting materials.

There is a long history of imitating the functions of animals and plants living in desert areas to produce biomimetic materials for AWH applications. A variety of functional materials, such as amphiphilic surfaces and artificial cactus spines, have been developed for saturated (fog) water harvesting,[18−20] and some novel aerodynamic designs have been inspired by other surface morphologies. For example, Harris et al. reported a biomimetic structured surface for atmospheric saturated water harvesting inspired by the Stenocara beetle,[21] which has an irregular textured shell with hydrophilic sites on its hydrophobic shell background.[22−26] To mimic this unique structure, hydrophobic polystyrene (PS) and hydrophilic poly(4-vinylpyridine) (P4VP) were subsequently coated on a substrate to afford a dual-layered coating (Figure 2). Due to poor compatibility, the P4VP segments tend to minimize its contact areas with PS under high-temperature annealing, resulting in the connection among isolated P4VP spheres on top of the PS layer. This structure has the ability to gather small water droplets on the surface of the hydrophilic P4VP spheres, thus allowing the growth of water droplets. Finally, the growing water droplets flow to the freshwater container along the hydrophobic PS surface under gravity. As expected, the water collection rate depended on the flow rate of the humid air. A condensation rate of 3400 mL m^{-2} h^{-1} was achieved at an air flow rate of 9.8 L min^{-1}. The amphiphilic surface presented the highest condensation rate compared to its pure PS or P4VP counterparts. Using a similar concept, a hybrid surface consisting of a surface covered by fluoroalkyl silanes (FAS) modified with TiO_2 and SiO_2 nanoparticles (NPs) was developed by Zhang's group.[27] The exposure to UV irradiation made the modified TiO_2 NPs become hydrophilic and dispersed on the surface discontinuously, while the SiO_2 NPs remained hydrophobic and were continuously arranged on the surface. These NPs, with a staggered arrangement and hydrophilicity, enabled the resulting surface to collect water droplets in the air. The hydrophilic small regions promoted the formation of water droplets, while the hydrophobic areas promoted the fusion and flow of grown droplets. As a result, this amphiphilic surface

https://doi.org/10.1021/acsmaterialsau.2c00027
ACS Mater. Au XXXX, XXX, XXX−XXX

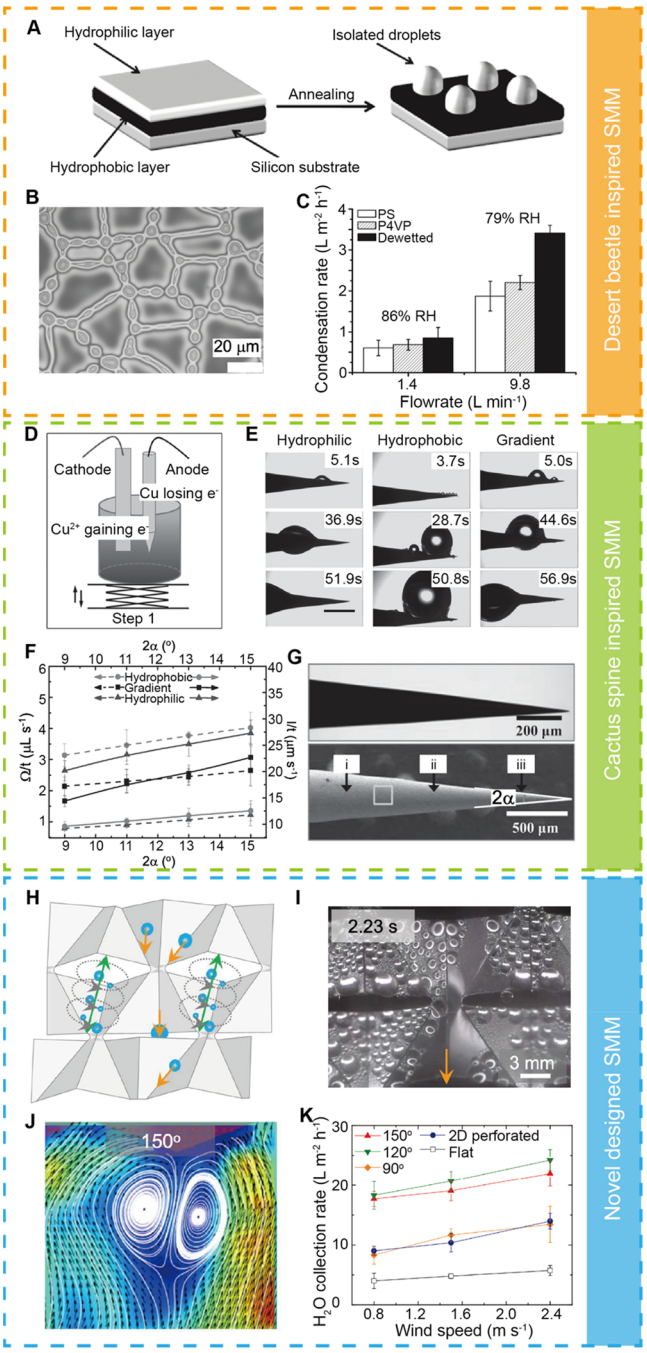

Figure 2. (A) Illustration of the dual-layered saturated water harvesting membrane. The top layer (plate or isolated droplets) and the middle layer (black) are made of P4VP and hydrophobic PS, respectively. (B) Optical microscopy image of the dewetted P4VP solid droplets. The dark background is the hydrophobic PS layer. (C) Rate of fog condensation on pure hydrophilic P4VP surface, pure hydrophobic PS surface, and PS plate decorated with P4VP solid droplets at 1.4 and 9.8 L min^{-1} of humid air flow rate. (E) Electrodeposition process in CCW fabrication. (F) Simulation of the fogwater harvesting process for pure hydrophilic, pure hydrophobic, and gradient modified CCWs within a 60 s period. (G) Saturated water harvesting rate ($\mu L\ s^{-1}$) and water droplet moving velocity ($\mu m\ s^{-1}$) for pure hydrophilic, pure hydrophobic, and gradient modified CCWs. (H) SEM images of a CCW that has a hydrophilicity gradient between its hydrophilic wider end and hydrophobic narrow end. (I) Structural design of a karigami 3D surface using an Al-coated PET sheet and schematic of the formation of addy currents. (J) Standard optic photo of the water droplets formation on the surface of PET sheet. (K) Mathematical modeling of addy current at the surface of a karigami surface. (L) Saturated water harvesting rates changing with increased flow rate of moist air for the karigami surface with flat (180°), 90°, 120°, and 150° bending. Panels (A)−(C) are adapted with permission from ref 21. Copyright 2011 John Wiley & Sons. Panels (D)−(G) are adapted with permission from ref 35. Copyright 2013 John Wiley & Sons. Panels (H)−(K) are adapted with permission under a Creative Commons CC BY License from ref 42. Copyright 2021 Springer Nature.

showed a maximum water harvesting capacity of 1700 g m^{-2} h^{-1}. The overall harvesting efficiency was affected by the flow rate of humid air, the specific surface area, the density of the hydrophilic NPs, and the placement angle of the surface. The water production was further optimized by adjusting the droplet transfer process. Other saturated water (fog) harvesting surfaces made of asymmetric fibers,[28] polyacrylonitrile/poly(methyl methacrylate) (PAN/PMMA) nanocomposite fibers,[29] and polypropyene (PP) surface embedded with polydopamine NPs[30] have also been reported.

Unlike the 2D horizontal surface inspired by desert beetles, the vertical designed 3D water harvester that can efficiently condense and then transfer gaseous water in an oversaturate humidity environment has also received widespread attention.[31] The cone-shaped cactus spines are composed of 50% cellulose, and 50% lignin, arabinan, or other nonstructural polysaccharides, which provide the spine a high affinity to water molecules for collecting fog droplets in desert areas.[32−34] By mimicking the microstructure of the spine, in 2013, the Jiang group reported a conical copper wire (CCW) with an axial gradient wettability for saturated water harvesting[35] (Figure 2D−G). The CCWs were fabricated by gradient electrochemical corrosion followed by gradient surface modification using different alkanethiols. The hydrophobic surface at the narrow end of the CCW (region F, Figure 2G) is conducive to the growth of small water droplets, while the hydrophilic surface at the wider end (region D, Figure 2G) can promote a greater difference in contact angle as the driving force for the movement of water droplets. The resultant CCW spine with gradient amphiphilicity exhibited a higher saturated water harvesting rate (2.5 $\mu L\ s^{-1}$) and a faster droplet moving velocity (22.5 $\mu m\ s^{-1}$) compared to its hydrophobic and hydrophilic counterparts. Similarly, a branched wire consisting of a large ZnO stem and an array of small ZnO branches was developed by the Luo group.[36] All the branched wires are conical in shape with gradually increasing diameters from the tip to the root, leading to a gradient capillary force for water collection. Through a magnetorheological drawing lithography method, Yi et al. fabricated a series of conical spines with backward-, vertical- and forward-facing microbarbs.[37] The conical spine with backward barbs can promote one-way transmission of water droplets and achieve a high saturated water harvesting efficiency due to its high Laplace pressure gradient and capillary pressure. Other similar systems, such as a multiple magnetic conical array,[38,39] spine-membrane integrated system,[40] and multipattern spine brush[41] have been also reported in the past few years. Unfortunately, it is difficult to compare the capacity and condensation rate of these saturated water harvesters due to their different shapes, sizes, and morphologies. Nevertheless, it is still possible to conclude that these designs are tightly optimized around the dynamics of the

https://doi.org/10.1021/acsmaterialsau.2c00027
ACS Mater. Au XXXX, XXX, XXX−XXX

Table 1. Representative Research Outcomes of Saturated Water Harvesting Materials

material	preparation method	character	capacity/rate	year	ref
PS, P4VP	spin-coating	staggered hydrophilic-phobic arrangement	0.17 L m^{-2} h^{-1}	2011	21
TiO_2, SiO_2 fluoroalkyl silane	UV-irradiated fabrication	hybrid superwettable surface	1.75 L m^{-2} h^{-1}	2018	27
		composite material			
PDMS, alginate	microfluidic controlled fabrication	inspired by desert beetle	39.24 L m^{-2} h^{-1}	2021	28
	3D-printing	asymmetric arrangement			
PAN, PMMA	electrospinning	composite material	6 L m^{-2} h^{-1}	2020	29
TiO_2, Al-NPs		TiO_2 NPs embedded			
PDA, SU-8 polymer	negative photolithograph	multilayered design	0.97 L m^{-2} h^{-1}	2017	30
ZnO	vapor phase approach	manipulated branched nanowire array	12 μL h^{-1}	2014	36
PDMS, Co-NPs	magnet-assisted molding	magnetic responsible	84 μL h^{-1}	2015	38
		spine direction controllable			
MPAM, MPs	magnet-assisted molding	IR heating fabrication	10.84 L m^{-2} h^{-1}	2013	39
		magnetic responsible			
Al, PET	electrodeposition	Janus membrane with hydrophobic (inside) and hydrophilic (outside) surface	3.3 L h^{-1}	2018	40
PMHS, Al	spray-coating	arc, triangle, and rectangle shape array	4.5 L m^{-2} h^{-1}	2021	41

droplet movement based on the Laplace pressure difference. As an example, the conical spine array responsive to a magnetic field relies on the movement of an external magnet in the static moist air to force the soft spine to bend, thereby accelerating the fusion and movement of water droplets. However, the movement of the magnet is difficult to conduct spontaneously, which limits the practical application of the device mentioned above. On the other hand, the integrated spine−membrane system has a better effect on the continuous flow of saturated gaseous water, in which water can be transferred to the membrane by air movement and subsequently move along the membrane via gravity. However, the currently reported spine objectives are fabricated by lab-scale inversion modeling or electrochemical corrosion and their manufacturing on a large scale (e.g., via 3D printing) is still a challenge.

So far, the main bottleneck affecting the harvesting of saturated water is the contact pattern between the humid air and the conical spine, that is, the aerodynamics and fluid mechanics of the humid air near the material surface. Inspired by eddy currents, Yang et al. conducted a new exploration of the surface morphology of water harvesting materials and created a kirigami-like 3D surface that promoted the generation of eddy currents in moist air, accelerated fog harvesting, and achieved an ultrahigh fog harvesting rate of 24.5 L m^{-1} h^{-1} at a moist air flow rate of 2.4 m s^{-1}. In this study, ultrathin Al-coated PET sheets (thickness = 127 μm) were employed to cut into the desired karigami-like 3D surface (Figure 2H−K). They fully evaluated the water harvesting rate of the 3D surface when the bending angles on the surface are flat (180°), 90°, 120°, and 150° and the humid air (0.8−2.4 m s^{-1}) flows perpendicular to the plane of the surface. The generation of eddy currents was also proved by mathematical modeling. As a result, this kirigami-like 3D surface achieves percent higher fog collection efficiency than those of all of the published structure surface materials for saturated water harvesting.[42]

Since water droplets tend to condense on hydrophilic surfaces and move on hydrophobic surfaces, the water collection designs described above, inspired by the desert beetle and cactus spine, are the mainstream designs for saturated atmospheric water harvesters. However, the water harvesting capacity and condensation rate achieved by different designs are different, which can be attributed to factors such as differences in the chemical structures of the surfaces and density of the conical spines. During the continuous growth and transfer of water droplets, it is extremely important to avoid the accumulation of water molecules in the microstructure on the surface, because the residual water covering the surface directly affects water harvesting efficiency and water droplet transfer kinetics. The biomimic conical spines have the characteristics of neat arrangement, consistent orientation, and single shape. The manufacturing cost of using small abrasives is high, which is not conducive to their commercial application. Therefore, the production of biomimic conical spines based on 3D printing technology becomes a potential solution. In 2020, Wang et al. successfully fabricated closely arranged Janus spines (half cones and half planes, inspired by the aloe vera plant) through projection micro-stereolithography 3D printing technology and revealed the growth and transport mechanism of water droplets.[43] This also provides a new idea for the development of next-generation air-saturated water harvesting materials.

The representative studies of saturated atmospheric water harvesting materials and their performance are provided in Table 1. It is found that the 3D printed PDMS/alginate-based materials displayed the highest saturated water collection rate of 39.24 L m^{-2} h^{-1} due to their hump-valley surface that is regularly arranged by microfluidic production. In addition, the metal oxides (ZnO) showed an insufficient collection rate of 12 μL h^{-1}. This result is attributed to the overcrowded branched nanowire array, which hindered the flow of liquid water. It can be seen that, to obtain higher water production rates for saturated water-harvesting materials, surface morphology design and appropriate surface modification should be combined.

There are also other challenges in the field of AWH materials. For instance, the structured surface materials commonly applied in saturated water harvesting have mainly two design directions: arranging hydrophilic functional patterns on the hydrophobic surface to achieve vapor condensation and water transport; and creating conical spines with gradient hydrophilicity (gradient Laplace pressure). Although lab-scale experiments have achieved an average water harvesting capacity of 3 g g^{-1}, there are still challenges in industrial-scale water production due to difficulties in the complicated manufacturing processes mainly associated with

https://doi.org/10.1021/acsmaterialsau.2c00027
ACS Mater. Au XXXX, XXX, XXX−XXX

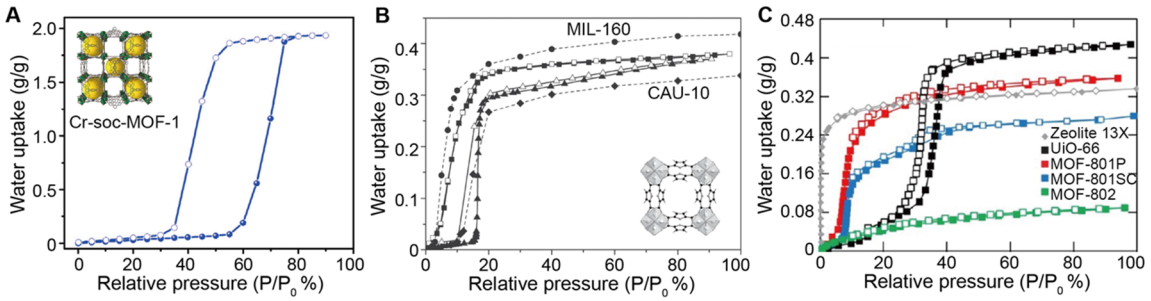

Figure 3. MOF water harvesters. Panel (A) is adapted with permission from ref 116. Copyright 2018 Elsevier. Panel (B) is adapted with permission from ref 113. Copyright 2015 John Wiley & Sons. Panel (C) is adapted from ref 58. Copyright 2014 American Chemical Society.

controlling the direction, length, and gradient hydrophilicity of the spines and the relatively high costs. However, it is expected that the gradually maturing 3D printing technology can resolve the aforementioned problems and produce cost-effective, long-term stable water harvesting systems. In addition, water transport on the material surface (e.g., a groove connected to the spine) is also important for reducing residual water and improving water collection efficiency.

3. UNSATURATED WATER HARVESTING

The water harvesting materials mentioned previously are able to capture supersaturated moisture droplets in the air (>100% RH). However, oversaturated water vapor is not always available due to difficulties associated with the temperature below the dew point. Therefore, research interests have been focused mostly on unsaturated water harvesting, i.e., collecting water molecules from the ambient environment. Without a doubt, this process is more complicated than saturated water harvesting, because it requires novel hydrophilic materials as well as different driving forces capable of effectively inducing water condensation and transfer. In general, atmospheric water harvesting can be achieved in two ways: passive and active water collection. For instance, hygroscopic materials can directly adsorb water molecules from moist air (unsaturated water) at any temperature. After actively cooling captured water by using an electricity-driven condenser, the unsaturated moist air reaches its dew point and is liquefied for collection (active dewing). The adsorbed water can also be liquefied at a low temperature (below the dew point temperature) at night, namely, passive dewing, by the adsorption of water droplets from moist air in the (super)saturated state on the surface of a cold and hydrophilic material surface. So far, active dewing devices with wind power generation and a variety of water adsorption beds with different physical structures have been proposed.[44,45] These devices rely on the unique structure and/or external energy to achieve atmospheric water harvesting and have achieved outstanding outcomes. In this section, we focus on spontaneous unsaturated water harvesting materials (including MOFs, HICs and derivatives, ILs, and functional hydrogels) for passive dewing and direct water molecule adsorption and discuss their structure−property−performance relationships from the perspective of materials chemistry. These materials invariably contain strong polar ionic bonds, coordination bonds, or functional groups, which are key to attracting polar water molecules. The cavities within the structure of these materials allow water molecules to adsorb, condense, and flow with gravity and surface tension from the surface to the interior, where the water ultimately stored. The captured water can be collected by two approaches: the evaporation−condensation process and direct extraction resulting from the shrinkage/deformation of hydrogels by environmental stimulation. Thus, large electrical devices are out of the scope of this Review.

3.1. Metal−Organic Frameworks (MOFs)

MOFs are a subclass of coordination polymers consisting of metal ions/clusters and organic ligands (also known as metal cluster linkers) connected via coordination bonds.[46] Since the first report in 1997, MOFs have been widely applied in the fields of gas separation, hydrogen storage, drug delivery systems, catalysis, and chemotherapy.[47−51] Due to their high affinity for polar water molecules, porous MOF materials with diverse porous structures and enhanced water stability have exhibited great potential for wastewater treatment and heavy metal removal[52−55] (Figure 3).

MOF materials are usually powdered and can be used alone, as an additive, or as any part of a special design (such as a core−shell composite) for the adsorption, transport, and storage of water molecules. The metal ions in MOFs are connected to the surrounding organic structures by coordination bonds, which have strong polarity. The cavities in the MOF unit are of molecular size and have the ability to store water molecules. Water molecules are adsorbed from the material surface and subsequently attracted to the cavity by the polar MOF units. Therefore, a portion of the water molecules will remain inside the cavity during desorption, which has a potential adverse effect on the desorption efficiency. However, MOF materials have the ability to adsorb water molecules in a low-humidity environment and thus have attracted much attention in the field of AWH. In 2017, Wang et al. developed MOF-801 [$Zr_6O_4(OH)_4$(fumarate)$_6$] and proved its potential for harvesting unsaturated atmospheric water for the first time (Figure 4A).[56] Thereafter, more than 20 types of MOF materials have been developed for atmospheric water harvesting applications.[57] MOF-801 was selected as the preferred material due to its well-recognized outstanding water adsorption behavior and high chemical stability (Figure 4C). The unsaturated water vapor can be introduced into the three cavities inside the secondary building units (Figure 4D) in a vacuum container to achieve water adsorption. MOF-801 has shown a water adsorption capacity of 0.4 g of water per g of dry MOF (i.e., g g^{-1}) at 90% RH and 0.28 g g^{-1} under 20% RH (Figure 4B), which is the highest capacity compared with other MOF materials, such as MOF-841, UiO-66, and PIZOF-2. Under medium RH conditions (26−75%), MOF-841 has also shown the highest capacity, while PIZOF-2 has exhibited a greater water adsorption capacity at the high RH region (>80%). In a separate study, the water uptake of MOF-based materials is proved to be proportionally correlated with their

https://doi.org/10.1021/acsmaterialsau.2c00027
ACS Mater. Au XXXX, XXX, XXX−XXX

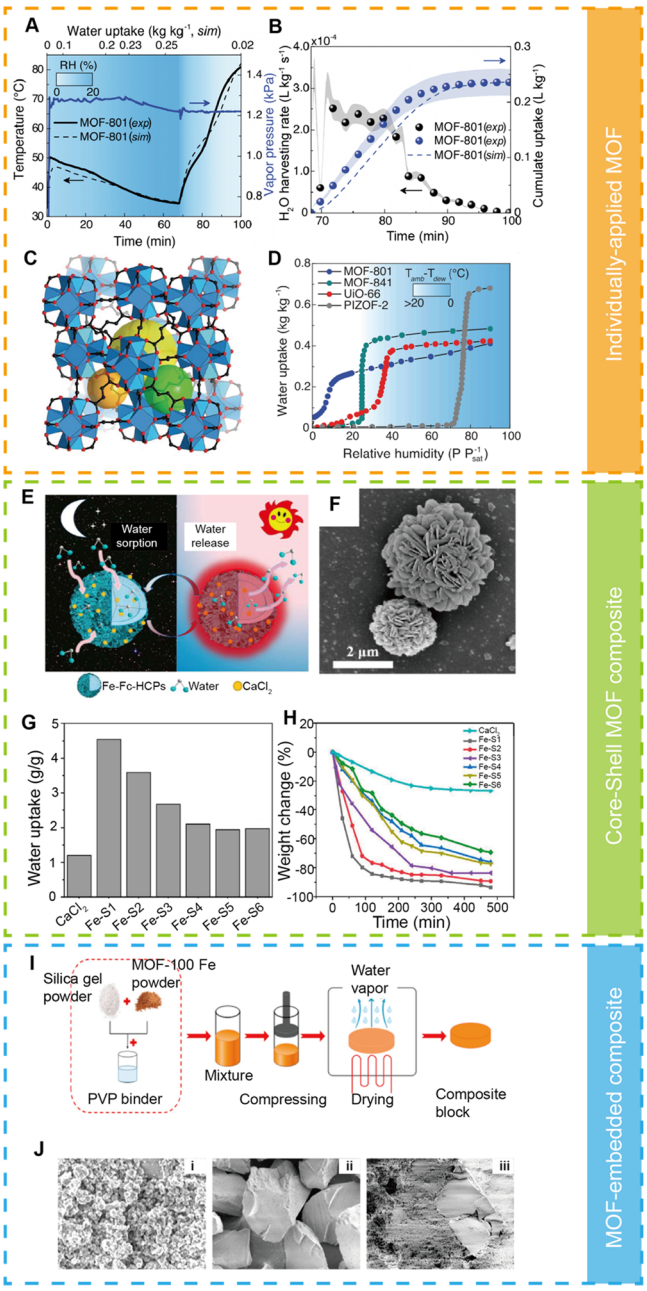

Figure 4. (A) Illustration of AWH system with forced thermoelectric (TE) cooler. (C) Schematic of the structure of MOF-801, with three porous areas (green, orange, and yellow spheres). Black and red dots refer to carbon and oxygen atoms, respectively. The Zr atom is located at the center of each blue polyhedral. (D) Atmospheric water harvesting isotherms of MOF-801, MOF-841, UiO-66, and PIZOF-2. (E) Atmospheric water harvesting and sunlight-induced water release mechanism. (F) SEM images of Fe-ferrocene MOF microspheres. (G) Temperature profile of Fe-S1, Fe-S2, Fe-S3, Fe-S4, Fe-S5, and Fe-S6 under 1.0 sun irradiation within 600 min. (H) Water loss capacity of Fe-S1, Fe-S2, Fe-S3, Fe-S4, Fe-S5, Fe-S6, and pure $CaCl_2$ under 1.0 sun irradiation within 500 min. (I) Manufacture procedure of SiO_2-MOF hybrid material. (J) SEM images of MIL-100(Fe) (i), silica gel (ii), and SiO_2-MOF hybrid material (iii). Panels (A)−(D) are adapted with permission from ref 56. Copyright 2017 The American Association for the Advancement of Science. Panels (E)−(H) are adapted with permission from ref 66. Copyright 2021 Elsevier. Panels (I) and (J) are adapted with permission from ref 68. Copyright 2021 Elsevier.

pore size and Langmuir surface area.[58] The larger surface area provides more opportunity for the water molecules to enter the MOF cavities, while the larger cavity size leads to less water transfer resistance, benefiting the water adsorption capacity. The cavity connection is controlled by the MOF topology, which is also related to the water adsorption kinetics. As an example, MOF-808 with "spn" topology has seven small cavities surrounding a large cavity. Its water uptake is doubled compared to that of MOF-805/806 ("fcu" topology) with a larger average cavity size.[58,59] Other water adsorption MOFs with different topologies have been reported elsewhere.[60−65] Although MOF-based materials with porous secondary building units have strong water affinity, the water adsorption capacity is still not sufficient for large scale water production. The exploration of MOF-based composite materials with greater water adsorption capacity and stimuli-response (i.e., thermal-induced) water release have greater potential for practical applications.

In order to improve photothermal conversion and achieve a thermal-induced water self-release, Hu et al. recently developed a novel composite microsphere with a MOF shell decorated with Fe-ferrocene groups, which encapsulated calcium chloride ($CaCl_2$) (Figure 4E−H).[66] The microsphere was synthesized by mixing iron(III) chloride and 1,1′-ferrocenedicarboxylic acid under high temperature and pressure using an autoclave, and the obtained MOF microspheres were then immersed into $CaCl_2$ solution that allowed the $CaCl_2$ molecules to enter the microspheres. Under 1 kW m^{-2} simulated sunlight irradiation for 10 min, the resultant composite microspheres exhibited a rapid temperature response and reached 62 °C (maximum). In addition, the composite microspheres incorporated a high-water adsorption of MOF and $CaCl_2$ which allowed them to achieve a maximum atmospheric water adsorption capacity of 4.54 g g^{-1} in an 80% RH environment and a self-release of 94% of contained water within 8 h under sunlight (Figure 4G). The only concern is that the loaded $CaCl_2$ may be leached from the MOF under extremely humid conditions or during the water release process. Using this "divide and conquer" strategy, the Maspoch group reported a MOF/poly(vinylidene difluoride) (PVDF) composite film.[67] With the assistance of the swellable structure of MIL-88A, the swellable MIL-88A on a dark PVDF sheet was assembled by chemical etching in order to form a variety of arrangements and prevent the film from curling due to the shrinkage and expansion of MIL-88A. It has been demonstrated that the combination of MOF and HICs could significantly increase the water adsorption capacity of AWH materials from less than 1g g^{-1} (using pure MOF) to around 3 g g^{-1} and achieve greater water release efficiency. However, bonding two materials together is challenging. Due to the different connection methods, the bonding materials have the potential risk of detachment or deformation. The encapsulation material also faces the risk of leakage of the encapsulated content. Different from a layered and encapsulation material, the uniform mixing of two (or more than two) materials has become a new design direction of AWH materials as an alternative to the other two approaches.

In the above study, the fabrication of the HIC loaded MOF materials is complicated and the HIC crystal may also cause leaching under high humidity conditions. To prevent these issues, the Maher group incorporated hygroscopic MIL-100(Fe) into inexpensive silica gel in the presence of a small amount of polyvinylpyrrolidone (PVP) binder and successfully prepared hybrid particles with a water adsorption of 0.56 g g^{-1}

https://doi.org/10.1021/acsmaterialsau.2c00027
ACS Mater. Au XXXX, XXX, XXX−XXX

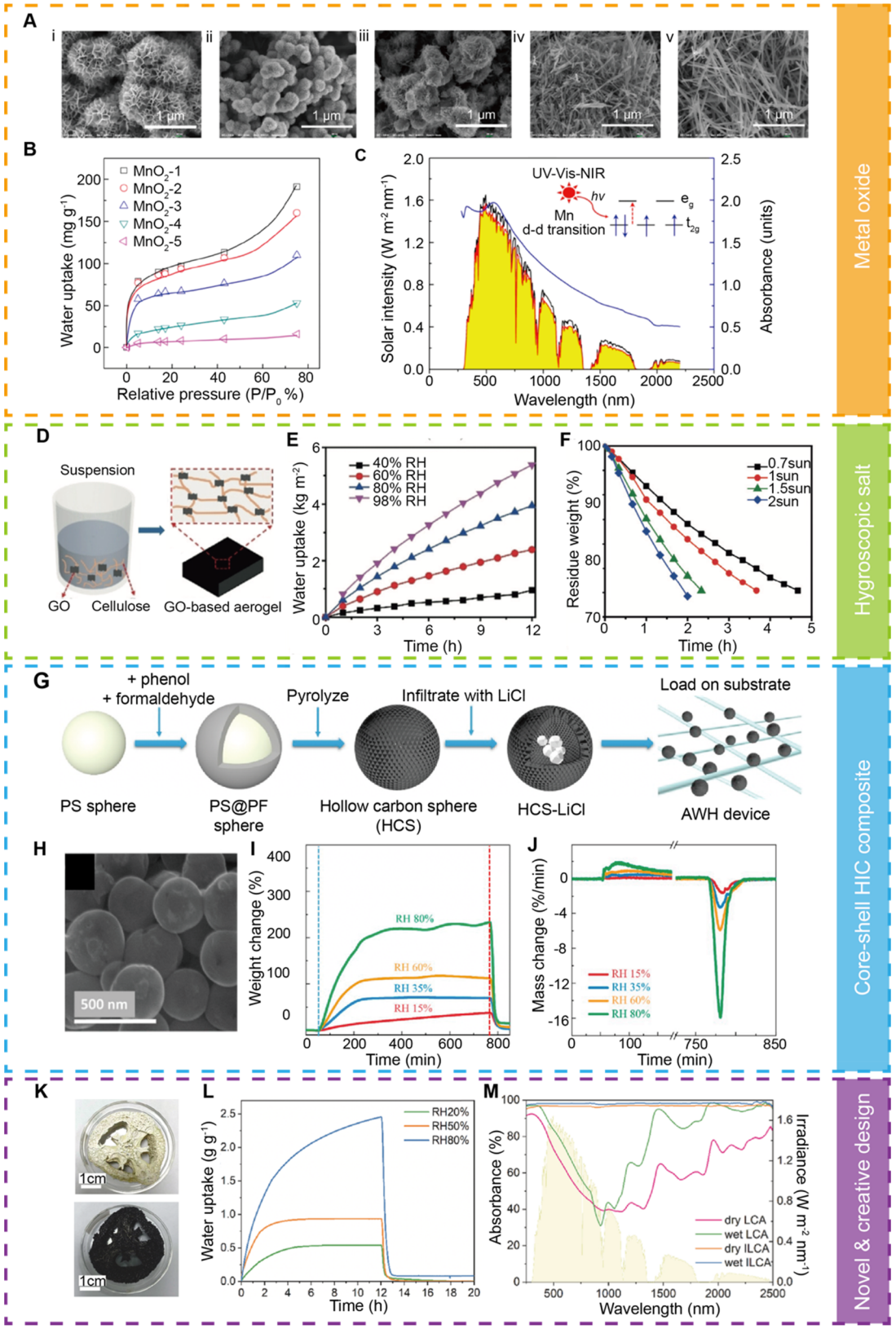

Figure 5. (A) SEM images of MnO_2 particles. Left to Right: pure birnessite to pure cryptomelane (MnO_2-1, MnO_2-2, MnO_2-3, MnO_2-4, MnO_2-5). (B) Atmospheric water adsorption isotherms for the five MnO_2 samples at 25 °C. (C) Equipment illustration of practical AWH system using MnO_2-1 sample. (D) Schematic of the synthesis of a graphene oxide based photothermal conversion film. (E) Water adsorption capacity of $CaCl_2$ solution at 40%, 60%, 80%, and 98% RH at 25 °C. (F) Water evaporation percentage of a $CaCl_2$ solution with graphene-oxide-based film at 0.7, 1.0, 1.5, and 2.0 sun equivalent irradiation. (G) Schematic of HCS-LiCl nanoscale sorbent. (H) SEM image of HCS-LiCl nanoparticle sorbent. (I) Adsorption and desorption behavior of HCS-LiCl nanoparticle sorbent. (J) Weight change and temperature profile of HCS-LiCl nanoparticle sorbent. (K) Morphology of loofah with SA matrix cross-linked inside the loofah structure (LCA) (i) and morphology of loofah with SA matrix

https://doi.org/10.1021/acsmaterialsau.2c00027
ACS Mater. Au XXXX, XXX, XXX−XXX

Figure 5. continued

cross-linked inside and SA+carbon covered outside of the loofah (ILCA) (ii). (L) Water uptake of SA and carbon modified loofah material in simultaneous thermal analyzer (STA). (M) Absorbance of the modified loofah sponge with wet and dry state. Panels (A)−(C) are adapted from ref 73. Copyright 2020 American Chemical Society. Panels (D)−(F) are adapted with permission from ref 75. Copyright 2019 John Wiley & Sons. Panels (G)−(J) are adapted with permission from ref 78. Copyright 2020 Elsevier. Panels (K)−M) are adapted with permission from ref 79. Copyright 2021 Elsevier.

under 90% RH conditions.[68] A further study indicated that the moisture adsorption under RH > 40% is positively linearly correlated with the mass ratio of MIL-100(Fe). It should be noted that under RH < 30% MIL-100(Fe) and silica gel had the same water adsorption capacity (Figure 4I−J). Notably, the addition of hygroscopic silica gel can significantly reduce the capital costs and maintain shape stability. Li's group incorporated black MXene Ti_3C_2 nanosheets into cylindrical monoliths composed of UiO-66-NH_2 for AWH applications.[69] This hybrid material achieved a maximum water adsorption of 0.23 g g^{-1} under 20% RH conditions and had the ability to release 50% of the captured water under the exposure of 1.0 sun equivalent irradiation within 30 min. However, the maximum water release is limited to 60% of the captured water and a large amount of residual water remains in the MOF building units, indicating insufficient driving force (heat) for evaporation. In other studies, MOF-based AWH hybrids, such as metal foam/MOF[70] and PNIPAM/MOF,[71] were also reported with good water collection ability (0.6−3.8 g g^{-1}). The water adsorption performance of MOF-based composites can be adjusted by varying the type of MOF, the hydrophilicity of the additives, and the ratio of MOF to additives. A greater proportion of MOF suggests more hydrophilic sites on the surface of the material, leading to great water affinity and better water adsorption capacity, and vice versa. One of the challenges of AWH hybrids is how to enhance the interfacial compatibility between different components and prevent possible deformation and/or decomposition under practical conditions.

So far, MOF-based AWH materials can achieve adsorption and storage of water molecules from low 10−20% RH to high 80−90% RH. Their hygroscopic ability still has room for improvement compared to that of hygroscopic salts and customized hydrogels. Moreover, the residual water in the MOF cavity is one of the bottlenecks restricting its AWH application. Therefore, research attention has been gradually redirected to MOF−polymer composite materials to maintain the high specific surface area and improve response to external stimuli (e.g., sunlight, electromagnetic coils), thereby achieving high reusability and water self-release. At the same time, efforts are focused on reducing the amount of water remaining in the MOF cavities to achieve further optimized release.

3.2. Hygroscopic Inorganic Compounds and Derivatives (HICs and Derivatives)

The hygroscopicity of inorganic compounds and derivatives (HICs and derivatives) describes their ability to take up atmospheric water from the environment. The adsorbed water molecules are not involved in the construction of crystal lattices and hence can be reversibly released under stimuli. The most widely used hygroscopic compounds are inorganic salts and metal oxides, which contain ionic bonds (cation−anion) and covalent bonds, respectively. These polar bonds can interact with water molecules through electrostatic attraction, resulting in the hygroscopic property or deliquescent phenomenon. In detail, HICs play the role of liquefying water vapor in sorption-based AWH materials. When used independently, water molecules can be attracted to the HIC surface through strong intermolecular forces, forming a layer of HIC solution. The lower vapor pressure of a hygroscopic salt solution tends to keep the water molecules in the solution rather than volatilize into the gas phase. Then, the liquid water is transported to the interior of HICs through the voids by capillary force and stored in them. The application of inorganic water sorbents for atmospheric water harvesting can be tracked back to 1998, when Gordeeva et al. reported the use of a fixed bed containing water sorbents (i.e., $CaCl_2$ and LiBr) to collect water from moist air.[72] Then the adsorbed water was evaporated and condensed for collection. With 20 years of development, this process is still one of the basic design strategies of modern AWH systems. Recently, Wang et al. developed a series of manganese oxide (MnO_2) particles and proved their great potential in the application of AWH.[73] By tuning the ratio of birnessite and cryptomelane (two manganese ores with different manganese oxides), the authors synthesized a series of MnO_2 particles with different surface morphologies and lattice structures. Both brinessite-rich and cryptomelane-rich samples presented hydrophilic surfaces due to the exposure of oxygen and manganese vacancies, while their difference of water adsorption capacity was caused by surface morphology. The brinessite-rich MnO_2 water sorbent has the form of sheet stacked sphere, where a large amount of water molecules can be adsorbed to the surface due to the greater surface area and then transferred to the porous structure inside the spheres by capillary forces (Figure 5A−C). Notably, the water adsorption kinetics of MnO_2 particles is also affected by the surface hydrogen bonds, porosity, and capillary force inside the particles. The birnessite-based MnO_2-1 (Figure 5A) also shows great photothermal conversion efficiency due to its broad light absorption range of 300−2200 nm and its wrinkled surface morphology, which increases the surface area and reduces reflection. The difference between brinessite and cryptomelane is that the ratio and arrangement of manganese atoms and oxygen atoms is different due to the different valences of the manganese ions. This determines the lattice structure of manganese oxide, the density of surface metal sites, and the size and space shape of cavities. Therefore, another challenge of this material is to prevent birnessite-based MnO_2 from being reduced to cryptomelane with a lower valence of manganese.

Hygroscopic salts have a strong dipole−dipole force that leads to a great water adsorption capacity (5−6 g g^{-1}).[74] However, the most severe drawback of these salts is that their powdery structure tends to agglomerate when exposed to water, resulting in low durability caused by a decrease in specific surface area. To maintain a continuous high water adsorption site density, hygroscopic salts are usually embedded in solid substrates or dispersed in liquid media for AWH applications. For example, Zhu et al. reported an AWH system using a high concentration (50 wt %) of calcium chloride

https://doi.org/10.1021/acsmaterialsau.2c00027
ACS Mater. Au XXXX, XXX, XXX−XXX

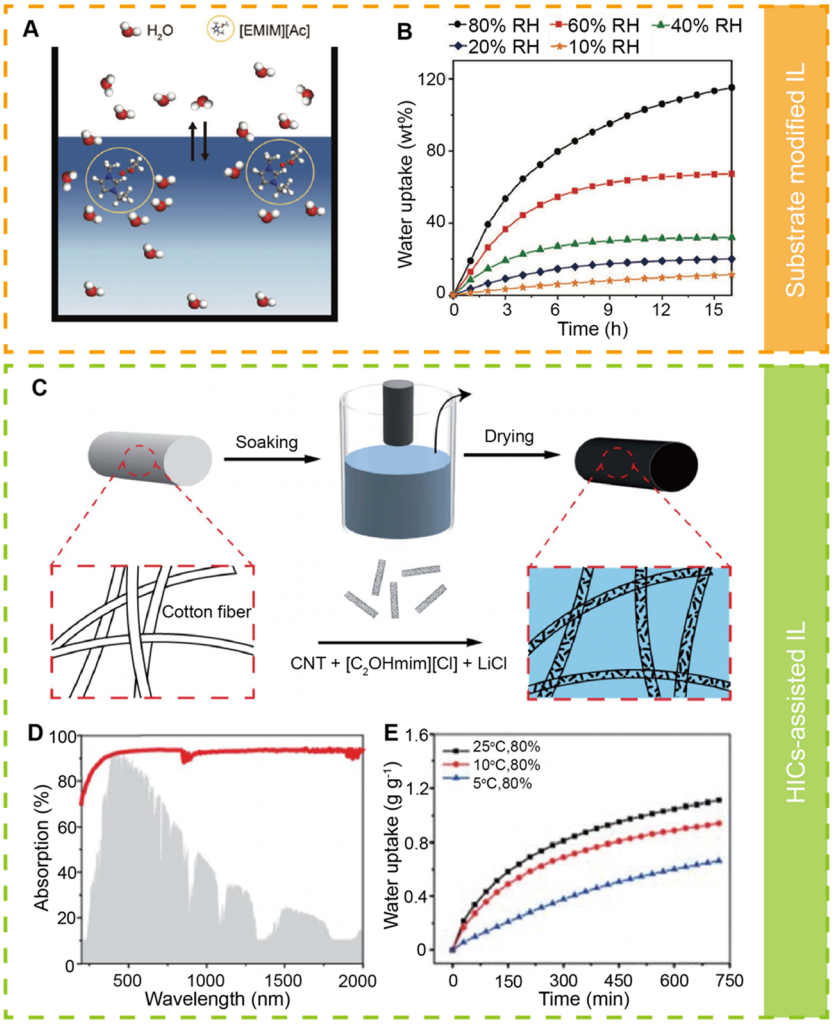

Figure 6. (A) Schematic of the water adsorption mechanism of [EMIM][Ac] ionic liquid. (B) Water adsorption capacity of [EMIM][Ac] ionic liquid at 10%, 20%, 40%, 60%, and 80% RH at 25 °C. (C) Schematic illustration of the fabrication procedure of the CNT-CILs@cotton rod. (D) UV−vis-NIR absorption spectrum of the CNT-CILs@cotton rod. (E) Static water adsorption curves of CILs at different temperatures under 80% RH. Panels (A) and (B) are adapted with permission from ref 88. Copyright 2019 John Wiley & Sons. Panels (C)−(E) are adapted with permission from ref 89. Copyright 2021 The Royal Society of Chemistry.

solution as the water adsorbent and placing a graphene oxide aerogel film on the surface of the solution for photothermal conversion to promote evaporation.[75] Due to the high water adsorption capacity of $CaCl_2$, a maximum water uptake of 5.3 kg m^{-2} (dividing the adsorbed water by the solution surface area) was achieved during night time. Thereafter, a graphene oxide/cellulose aerogel film was placed on the surface. Under daily sunlight irradiation, the temperature of the aerogel reached 60 °C, resulting in 70% contained water release within 4 h (Figure 5D−F). Similarly, Wang's group loaded LiCl and $MgSO_4$ on activated carbon fiber (ACF) films by submerging them in LiCl and $MgSO_4$ solutions, respectively, followed by oven drying. These materials achieved a maximum water uptake capacity of 2.3 g g^{-1} at 70% RH and released almost 100% of the adsorbed water within 3 h at 80 °C.[76] Compared to hygroscopic oxides, hygroscopic salts usually show higher water adsorption capacity, but they are light-colored. Therefore the application of strong hygroscopic salts requires the use of photothermal converters to achieve fast water release (usually, through evaporation). Moreover, due to the strong intermolecular forces between the hygroscopic salt and water molecules, the directly released water may contain dissolved salt ions. Thus, the release of water from hygroscopic salts mainly relies on thermally driven evaporation processes. Reports on similar studies can be found elsewhere.[77]

To address the structural fragility of HICs, many creative designs have been employed to embed HICs into encapsulation materials. As shown in Figure 5G and H, Wang's group prepared nanoscale hollow carbon spheres with an average diameter of 300 nm for encapsulating hygroscopic salt.[78] The resultant hybrid AWH material had a hygroscopic capacity of 2.3 g g^{-1} at 80% RH. Surprisingly, the carbon sphere can achieve an astonishing 91.3% water desorption efficiency within 1 h (Figure 5I). The same group reported another AWH material consisting of a sodium alginate (SA) matrix with $CaCl_2$ and modified loofah fiber support (Figure 5K).[79] The support material can absorb solar irradiation from 300 to 2500 nm (Figure 5M). This prepared AWH material had a water adsorption capacity of 2.45 g g^{-1} at 80% RH and 0.85 g g^{-1} at 50% RH (Figure 5L). Reports on similar studies can be found elsewhere.[80−83]

As the materials that inspired people to conduct AWH research, HICs have exhibited outstanding unsaturated water adsorption performance. However, HICs show low structural

https://doi.org/10.1021/acsmaterialsau.2c00027
ACS Mater. Au XXXX, XXX, XXX−XXX

stability, low resistance to ionization, and poor response to external stimuli, thus limiting their applications. In short, the application of HICs and derivatives faces two major bottlenecks: instability of crystal structure and limited response to environmental stimuli, which reduce the cycle performance and water release rate, respectively. Therefore, recent research has focused on the development of HIC-embedded hybrid materials such as HIC/MOF and HIC/ACF or SVG systems to overcome the aforementioned obstacles.

3.3. Ionic liquids (ILs)

Ionic liquids (ILs) are highly viscous fluids composed entirely of anions and cations. Chemicals linked by ionic bonds (e.g., sodium chloride, calcium carbonate, etc.) are usually solid because of the close distance between ions with stable ionic bonds. However, the volume difference between the anions and cations that make up the ionic liquid is large, where the electrostatic attraction cannot effectively connect them together, so that the anions and cations are in a free state then called "ionic liquid".[84] Similarly, ILs still adsorb water molecules through strong electrostatic attraction with water molecules. However, compared with HICs, the transport of water molecules from the surface to the interior of the ILs relies on concentration gradient-based diffusion. Since entering the field of scientists in 1914, ILs have been applied in the field of gas adsorption and as a substitute for organic solvents. In 2002, BASF first applied ILs to the biphasic acid scavenging process in chemical production.[85]

The idea of using ILs for AWH originated from its great potential in the field of gas adsorption. In 2002, Zhang et al. reported the application of ILs for efficient sulfur removal (SO_2 adsorption) from flue gas, which suggested its potential for water vapor adsorption.[86,87] In 2019, Zhu et al. reported a typical application of IL-based AWH.[88] In this work, an IL pair (1-ethyl-3-methyl-imidazolium cation $[EMIM]^+$/acetate anion $[Ac]^-$) was selected as a strong water vapor adsorbent (Figure 6A). The polar water molecules are connected to $[EMIM]^+$/$[Ac]^-$ through hydrogen bonds at the liquid surface and then flow toward the inside of the IL following the concentration gradient. With the increase of the adsorption capacity of water molecules, the bonding energy of the hydrogen bonds between water molecules and IL pair gradually decreased from 93.64 kJ mol^{-1} and stabilized at 53.99 kJ mol^{-1}, indicating that the adsorption of water molecules reached its maximum capacity of ca. 1.12 g g^{-1} (80% RH). However, this IL pair can only reach 0.18 and 0.1 g g^{-1} at low RHs of 20% and 10%, respectively (Figure 6B). Another IL-based AWH composite material is reported by Chen's group.[89] In this work, a composite IL consisting of $[C_2OHmim][Cl]$ and LiCl (in ethanol) was mixed with carbon nanotubes (CNTs; photothermal material). The mixture was then dispersed in cotton rods, followed by oven drying (Figure 6E). The resultant CNT-CILs@cotton rod presented a wide UV−vis-NIR absorption range (Figure 6F) and a high water adsorption capacity of 1.15 g g^{-1} at 25 °C and 80% RH (Figure 6G). This composite material also showed a maximum 2.0 kg m^{-2} h^{-1} water evaporation rate and 70% water-release efficiency under 1.0 sunlight irradiation. Similar research outcomes can be found elsewhere.[90]

Unfortunately, the strong affinity of IL materials for water vapor indicates that desorption of water molecules will be more difficult. In addition, the difficulties in transportation of ILs, higher weight compared with porous solid adsorbers, high residual water content, etc. have all become bottlenecks for their practical application in the field of AWH.

3.4. Functional Hydrogels

A hydrogel is a type of hydrophilic gel with a three-dimensional network structure. It can automatically expand its volume and hold a large amount of water without structural damage. In general, the network structure of a hydrogel is composed of "polymer chains" and "cross-linking points" with functional groups along with polymer segments. Due to the diversity of hydrogels, they can be classified in different ways. According to cross-linking methods, hydrogels can be divided into physically and chemically cross-linked gels.[91] Similarly, hydrogels can also be divided into natural hydrogels and synthetic hydrogels based on different raw materials used[92] or traditional hydrogels and stimuli-responsive hydrogels depending on the environmental stimulation.[93−96] Hydrogels applied in AWH are usually synthetic hydrogels of the stimuli-responsive type, allowing for controlled water release. Hydrogel-based AWH materials have unique advantages such as high design freedom, strong water adsorption capacity, and the ability to integrate autonomous water release function. The mechanism of water adsorption and transportation in AWH hydrogels are briefly shown in Figure 7. Specifically, the water

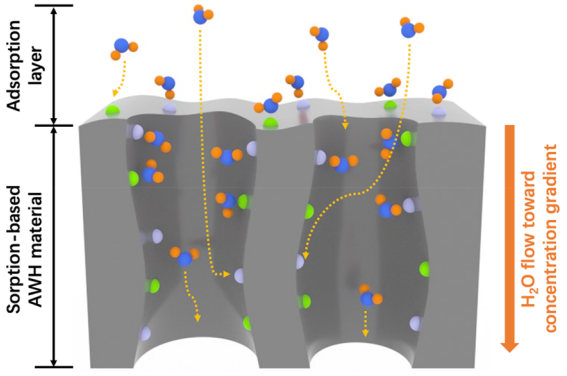

Figure 7. Schematic illustration of water adsorption mechanism of AWH hydrogel. (Green and purple dots: adsorption sites composed of hydrophilic functional groups.)

vapor can be adsorbed on the surface of the hydrogel, where the distribution of water molecules changes vertically and the adsorption layer is formed. Water molecules are then attracted and flow toward the "wall" of hydrogels and transport along the interconnected pores due to the capillary force and concentration gradient.

3.4.1. Hydrogels without Stimulus Response. A conventional composite hydrogel adsorbs water through the strong affinity between its functional groups and water molecules. Under sunlight irradiation, the embedded photothermal converter (fillers) induces temperature elevation and the adsorbed water molecules are released through evaporation. Such a material can only harvest liquid water when coupled to a supporting passive condensing device (such as an inclined glass plate connected to a liquid water collection container installed above the hydrogel), as the evaporated water vapor must be condensed before it is collected. Other additives (e.g., HICs) can also be added to such composite hydrogels to enhance their ability to attract and liquefy water.

As mentioned above, HICs with strong polarity have great attraction to water molecules, and the high swelling ratio of

https://doi.org/10.1021/acsmaterialsau.2c00027
ACS Mater. Au XXXX, XXX, XXX−XXX

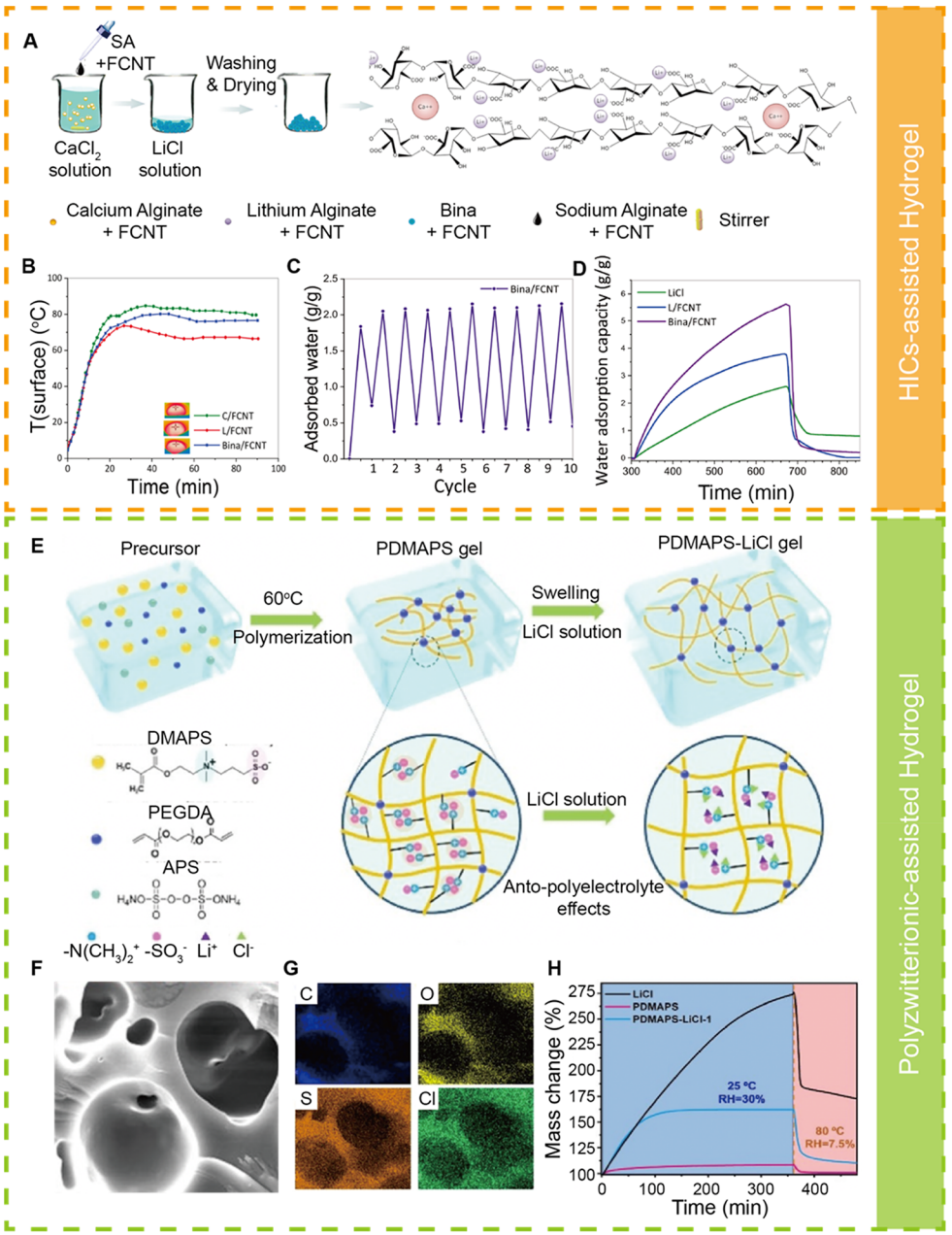

Figure 8. (A) Manufacture process of a Ca/Li-CNT hydrogel. (B) Water release temperature versus time for Ca-CNT, Li-CNT, and Ca/Li-CNT hydrogels. (C) Water adsorption-release cycle test. (D) Plots of moisture adsorption capacity variations within 800 min for LiCl, Li-CNT hydrogel, and Ca/Li-CNT hydrogel. (E) Illustration of the PDMAPS-LiCl hydrogel and its water adsorption mechanism. (F−G) SEM image and EDS mapping of PDMAPS-LiCl-1 hydrogel, respectively. (H) Sorption−desorption curves of pure LiCl (black), bare PDMAPS hydrogel (pink), and PDMAPS/LiCl hybrid system (blue). Panels (A)−(D) are adapted from ref 77. Copyright 2020 American Chemical Society. Panels (E)−(H) are adapted with permission from ref 105. Copyright 2022 John Wiley & Sons.

hydrogels is expected to play a key role for water storage. Therefore, HIC-assisted composite hydrogels can achieve the greatest water adsorption capacity of 5.4 g g^{-1}.[75] As an example, Wang et al. constructed an AWH composite hydrogel consisting of sodium alginate hydrogel as a carrier, functionalized multiwalled CNTs (FCNTs) as the photothermal converter, and HICs ($CaCl_2$ and LiCl) to improve adsorption capacity (Figure 8A−D).[77] This composite hydrogel achieved a maximum water adsorption capacity of 5.6 g g^{-1} at 90% RH using both $CaCl_2$ and LiCl, but with a slightly reduced sunlight absorption efficiency that may be due to the lower FCNT density.[97] The hydrogel with both $CaCl_2$ and LiCl reached approximately 75 °C for water release that was slightly lower than that of the $CaCl_2$ only hydrogel but higher than that of the LiCl only hydrogel. In a separate study, Ni's group reported a semi-interpenetrating gel by introducing polypyrrole-dopamine (P-Py-DA) into a poly(sodium methacrylate-*co*-acrylamide) (P(SMA-*co*-AM)) copolymeric network. The water within this gel was then replaced with glycerine, forming a hygroscopic photothermal organogel (POG) with a maximum moisture adsorption capacity of 0.6 g g^{-1}.[98] In this study, the water molecules adsorbed on the surface of the material can form stronger hydrogen bonds with the polymer chains, thereby replacing the bonding sites that previously

https://doi.org/10.1021/acsmaterialsau.2c00027
ACS Mater. Au XXXX, XXX, XXX−XXX

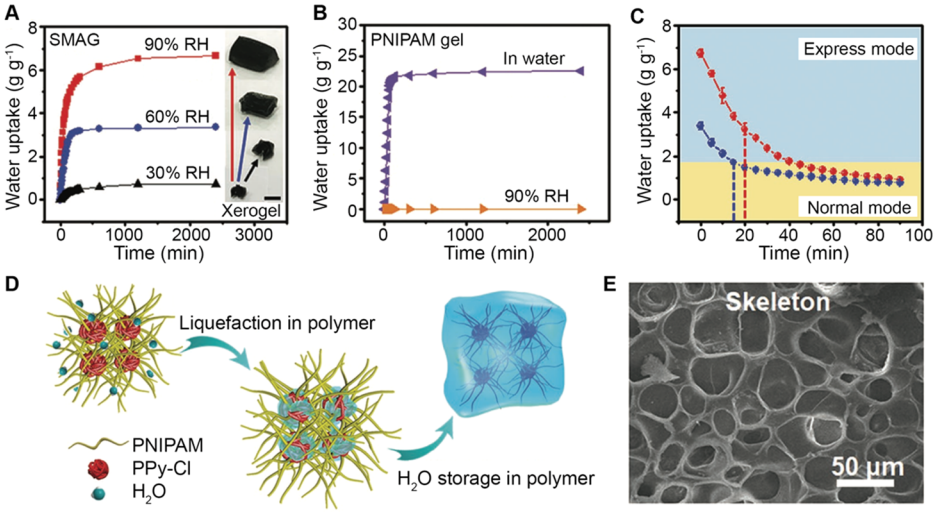

Figure 9. (A) Water uptake of PPy-Cl containing hydrogel versus time under different relative humidity (30%, 60%, and 90%). (B) Comparison of water uptake of PPy-Cl containing hydrogel versus time in a liquid water and moist environment. (C) Water release versus time of a PPy-Cl containing hydrogel. (D) Mechanism of water storage in a PPy-Cl containing hydrogel. (E) SEM image of a PPy-Cl containing hydrogel. Panels (A)−(E) are adapted with permission from ref 112. Copyright 2019 John Wiley & Sons.

attracted glycerol molecules. This process activated the adsorption sites on the polymer chains and provided a driving force for the following water molecule adsorption. In short, the use of hydrogels significantly improved the overall stability of AWH materials compared with MOF-based, powderlike materials. However, the process of releasing water from these conventional hydrogels relies on sunlight irradiation and the high temperature generated by embedded photothermal converters to evaporate the adsorbed water, which is then condensed by a cooling system for collection. Reports on similar hydrogel designs using photothermal converter and HICs as additives can be found elsewhere.[99−104]

More recently, Yu et al. reported the preparation of a polyzwitterionic (PDMAPS) hydrogel containing an immobilized hygroscopic salt (LiCl) by solvent replacement (Figure 8E−H).[105] The incorporation of highly polar LiCl is for the attraction and liquefaction of water molecules. The liquefied water forms a thin layer of LiCl solution on the surface, which can help realize the transport and storage of water. Compared with the bare PDMAPS hydrogel, the resulting hybrid gel showed a 3 times larger swelling ratio and 4 times higher unsaturated water harvesting capacity (0.62 g g^{-1}). This is the record high water adsorption capacity reported for a low RH region (30% RH). In addition, approximately 80% of the captured water (0.5 g g^{-1}) was released by evaporation at 80 °C within 0.5 h. This study demonstrates the high design freedom of polymer hydrogels, which enables HICs to be incorporated into hydrogel-based AWH systems to further enhance water adsorption. Similar progress using zwitterionic polymer as AWH water sorbent can be found elsewhere.[106]

3.4.2. Deformable Hydrogels with Environmental Stimuli Response. Poly(*N*-isopropylacrylamide) (PNIPAM) is one of the mostly used stimuli-response polymers,[107,108] with a lower critical solution temperature (LCST) of 37 °C,[109] which triggers the hydrophilic−hydrophobic transition. Specifically, under 37 °C, the amide group (−CONH−) of the NIPAM unit can display strong hydrogen bonding with water molecules, making the polymer water-soluble. When the temperature rises above 37 °C, the relatively weak bond energy (8−200 kJ/mol), compared to a common intramolecular bond of 200−1000 kJ/mol, makes the bond easy to break.[110,111] The hydrophobicity has a stronger effect than hydrophilicity, because the hydrogen bond between the amide group and water is too weak to offset the hydrophobic effect of the isopropyl group. Therefore, the dry PNIPAM-based hydrogel can automatically adsorb water when the temperature is lower than the LCST and release liquid water directly when the temperature is higher than the LCST, and thus, it has become one of the widely used materials to achieve spontaneous water release in AWH applications.

Photothermal converters have been introduced into PNIPAM-based hydrogels to elevate the temperature of the gel body, thus inducing gel volumetric contraction and water release.[94] In 2019, Yu et al. reported that the integration of high water adsorption capacity and self-contracting release can be achieved by incorporating polypyrrole chloride (PPy-Cl) into the PNIPAM hydrogel (Figure 9).[112] PPy-Cl, composed of numerous pyrrole rings, is able to absorb broad electromagnetic waves in the visible light band and convert it to heat. At the same time the NH^+/Cl^- charge pairs of polypyrrole can further increase the water adsorption capacity of the hydrogel due to their strong polarity. The water adsorption of the resultant composite material under RH 30%, 60%, and 90% can reach 0.7 g g^{-1}, 3.3 g g^{-1}, and an astonishing 6.6 g g^{-1}, respectively. Within 30 min, 50% of the adsorbed water can be released in an express mode, followed by a 60 min of normal mode to release the remaining 50%. Similarly, using PNIPAM as a carrier, Yilmaz's group designed a composite hydrogel consisting of Au nanoparticle loaded MIL-101(Cr) as a photothermal converter.[120] This composite gel showed a maximum water adsorption capacity of 3.0 g g^{-1} within 12 h at 90% RH. With the assistance of Au nanoparticles, this hydrogel reached 60 °C under 1.0 sun solar irradiation within 30 min. As a result, the hydrogel displayed an average water release efficiency of 93% under sunlight irradiation. With the addition of hydrogels, the water adsorption capacity of AWH materials has risen from less than 1 to 6−7 g g^{-1}, which means that hydrogel-based materials are currently the best materials in the field of atmospheric water harvesting. The addition of a photothermal converter gives the hydrogel material the ability

https://doi.org/10.1021/acsmaterialsau.2c00027
ACS Mater. Au XXXX, XXX, XXX−XXX

Table 2. List of the Sorption Based Unsaturated Awh Materials and Their Adsorption and Desorption Performance

type	material	ads. capacity (g g^{-1})[a]	des. capacity (g g^{-1})[b]	driving force	year	ref
MOF	MIL-160	0.39 (90% RH)		hydrogen bond MOF cavity	2015	113
	Ni_2Cl_2BTDD	1.1 (95% RH)	0.1 (30 °C*)	hydrogen bond MOF cavity	2019	114
	MOF-801	3.3 (40% RH)	2.3 (65 °C)	hydrogen bond MOF cavity	2018	115
	Cr-soc-MOF-1	1.9 (90% RH)	0.1 (25 °C*)	hydrogen bond MOF cavity	2018	116
	MOF-801	2.8 (20% RH)	0.02 (35 °C*)	hydrogen bond MOF cavity	2017	56
	Zr-fum-MOF	2.75 (90% RH)		hydrogen bond MOF cavity	2011	60
	DUT-67	2.7 (90% RH)	1.1 (25 °C*)	hydrogen bond MOF cavity	2013	61
	Fe-Fc-HCPs, $CaCl_2$	4.54 (80% RH)	4.3 (55−63 °C)	electromagnetic attraction hydrogen bond MOF cavity	2021	66
	HCS, LiCl	3.5 (80% RH)	2.5 (73 °C)	electromagnetic attraction	2020	78
	MIL-100(Fe), silica gel	0.7 (90% RH)	0.53(−)	hydrogen bond MOF cavity	2021	68
	UiO-66, T_3C_2, SA	0.7 (80% RH)	0.17 (70 °C)	hydrogen bond MOF cavity	2021	69
	MIL-101(Cr), SA	1.3 (90% RH)	0.6 (95 °C)	hydrogen bond MOF cavity	2021	70
HICs and derivatives	MnO_2	1.8 (80% RH)	0.26 (49 °C)	electromagnetic attraction conc. gradient	2020	73
	$CaCl_2$, GO	5.4 (98% RH)	3.89 (60 °C)	electromagnetic attraction conc. gradient	2019	75
	LiCl, ACFF	3.6 (90% RH)	2.1 (80 °C)	electromagnetic attraction conc. gradient	2021	117
IL[c]	[EMIM][Ac]	1.2	0.1 (70−90 °C)	electromagnetic attraction conc. gradient	2019	88
	SiO_2, TFSI, Si−P8	0.25		electromagnetic attraction conc. gradient	2019	118
function customized hydrogel	NIPAM, CNT, $CaCl_2$	1.75 (80% RH)	1.51 (75 °C)	conc. gradient electromagnetic attraction photothermal	2018	103
	Zn acetate, ethanolamine	3.7 (90% RH)	3.45 (55 °C)	conc. gradient photothermal	2019	119
	NIPAM, MIL-101Cr	3.5 (90% RH)	3.2 (61 °C)	conc. gradient MOF cavity photothermal	2020	120
	NIPAM, PPy-Cl	6.2 (90% RH)	5.9 (63 °C)	conc. gradient photothermal	2019	112
	alginate, $CaCl_2$, LiCl	5.6 (70% RH)	5.3 (72−75 °C)	electromagnetic attraction conc. gradient external energy	2020	97
	alginate, $CaCl_2$	0.8 (25% RH)	0.72 (100 °C)	electromagnetic attraction conc. gradient external energy	2018	99
	BSAMA	0.51(−)	0.44 (37 °C)	conc. gradient external energy	2018	101
	AEtMA, acetate	1 (85% RH)	0.9 (70 °C)	conc. gradient photothermal	2021	102
	AAm, PPy, dopamine	1.54 (90% RH)	1.33 (58 °C)	conc. gradient photothermal	2020	98
	PDMAP, LiCl	0.6 (30% RH)	0.5 (80 °C)	conc. gradient zwitterionic attraction	2022	105

[a]The reported relevant humidity is shown in parentheses. [b]The desorption temperature is shown in parentheses. [c]The value of desorption temperature with marked with an asterisk is obtained from adsorption−desorption isotherms, it is the experimental condition, and may not the temperature at which practical water release is triggered.

https://doi.org/10.1021/acsmaterialsau.2c00027
ACS Mater. Au XXXX, XXX, XXX−XXX

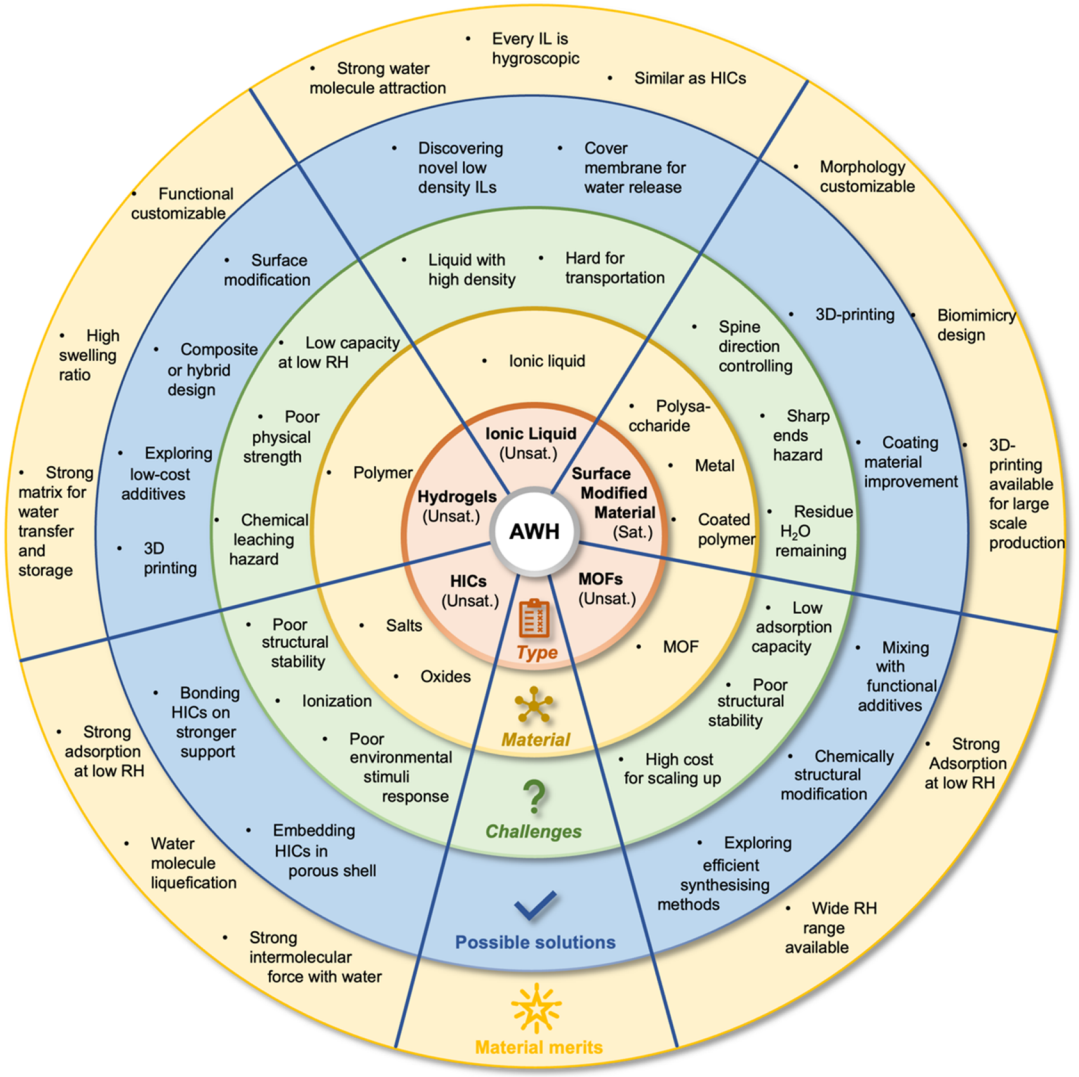

Figure 10. Application scene, existing challenges, and research directions of AWH materials. (Unsat: unsaturated water harvesting. Sat: saturated water harvesting.)

to quickly convert sunlight into heat energy, although it has been demonstrated to reduce the water adsorption capacity. In addition, the water adsorption kinetics of AWH hydrogels is still under investigation due to the differences in functional groups and polymeric network structures, which determines whether these materials have potential for harvesting water under unforeseeable conditions such as low humidity or a short time period. Reports on similar water harvesting designs can be found elsewhere.[71] The detailed comparison of the different AWH materials can be found in Table 2.

Hydrogel-based AWH materials are arguably the most promising option among AWH materials due to their customized functions and diversified additives for efficient water harvesting applications. Hydrogel materials have an excellent balance between their physical strength and AWH properties, but there is still potential for further improvement. So far, there is no sorption-based AWH material that can reach an adsorption capacity of 1 g g^{-1} at <30% RH, which has become the biggest bottleneck in the development of a sorption-based AWH system. Moreover, at low humidity, it is difficult for sorption-based materials to store liquefied water due to the dynamic balance between the liquefaction rate of water molecules on the surface of the material and the evaporation rate of liquid water.

4. CHALLENGES AND PERSPECTIVE

Water production using synthetic AWH materials (such as structured surface materials, HICs and derivatives, MOFs, and functional hydrogels) provides an alternative to conventional methods to solve the shortage of freshwater due to their portable size, high water harvesting capacity, lack of secondary energy requirement, and easy installation. Despite the continued great challenges in this field, the Google Earth Engine simulation data suggested that, by improving the design of water harvesting equipment and the type of adsorption materials, the existing water resources are fully capable of providing the global population 5 L of drinking water every day using AWH materials within the thermodynamic constraints in the foreseeable future.[121] As shown in Figure 10, we compared the advantages and disadvantages of different AWH materials and highlight the research challenges and potential solutions in this field. For future research, it is highly expected that researchers can focus on the combination of different types of AWH materials and the utilization of different diffusion

https://doi.org/10.1021/acsmaterialsau.2c00027
ACS Mater. Au XXXX, XXX, XXX−XXX

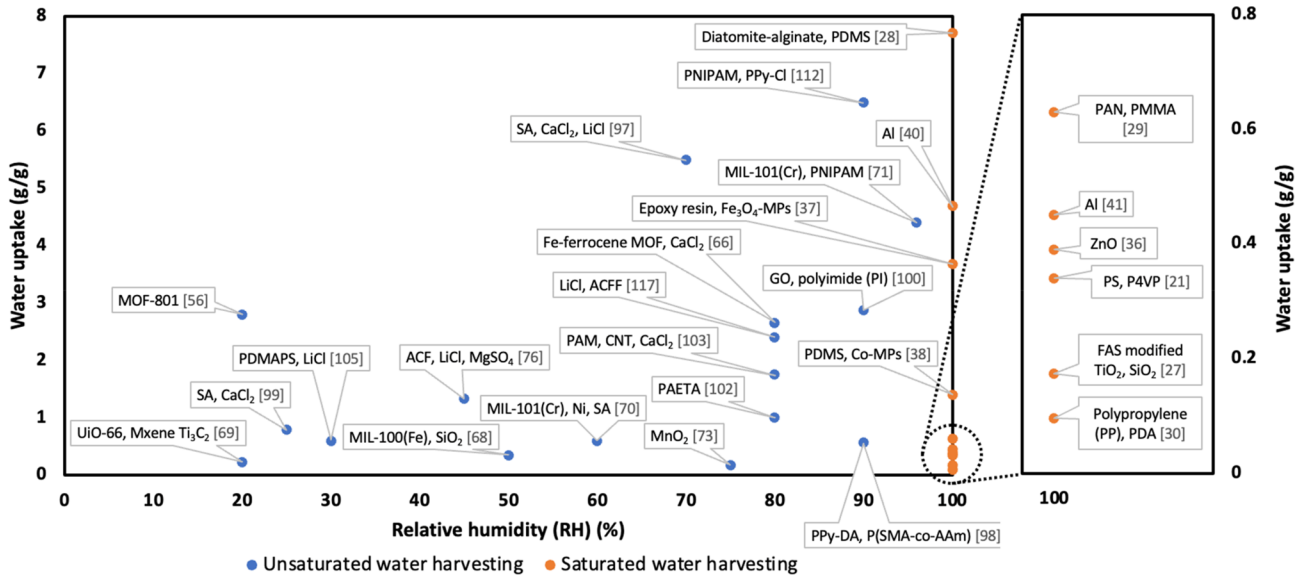

Figure 11. Summary of water harvesting capacity of AWH materials.

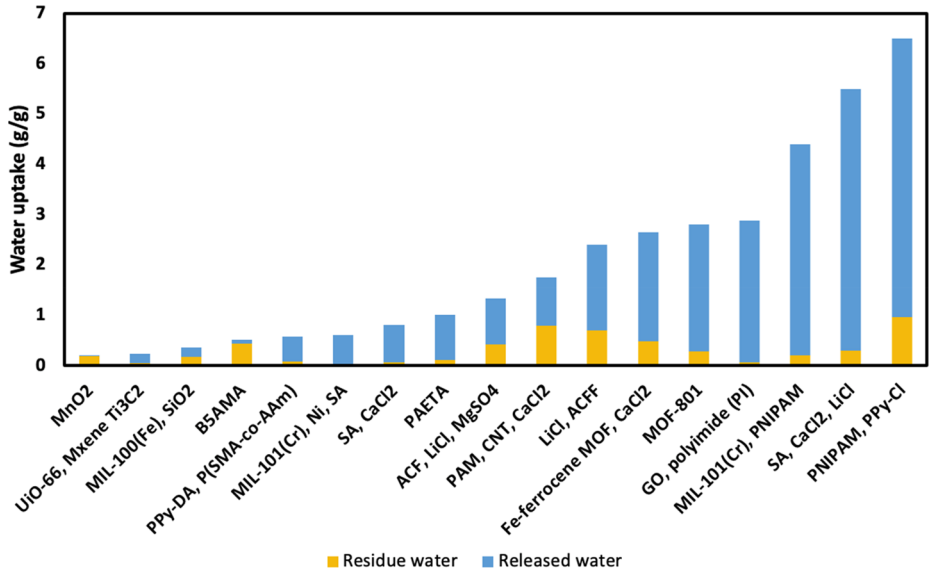

Figure 12. Water adsorption capacity and captured water release performance of AWH materials.

mechanisms to achieve greater water adsorption and desorption efficiencies.

Most sorption-based AWH materials present satisfactory adsorption capacities under high RH environments but unsatisfactory performance when the RH is lower than 60% (Figure 11).[70,99] Thus, compared with the active dewing process, the high adsorption capacity of current AWH materials in the high relative humidity region appears to have little advantage. Based on the characteristic that MOF materials have considerable water absorption capacity under medium and low humidity conditions,[56,68−70] the development of novel MOF−hydrogel composites through core−shell structures, customized MOF cavities, and other engineering solutions is expected to address the challenge of insufficient water absorption capacity of current AWH materials.

Recent research focuses on the development of new AWH materials to achieve higher water capture and/or production performance. For instance, the PNIPAM/PPy-Cl hydrogels displayed a high water collection capacity of 6.5 g g^{-1}[112] by regulating the affinity of the hydrogels and the H_2O diffusion dynamics (from the surface into the matrix). However, the high affinity of AWH materials for water molecules in turn restricts the rapid release of water from AWH materials (Figure 12). Although the incorporation of photothermal additives to AWH materials can facilitate water release through evaporation, their relatively lower hydrophilicity and incompatibility with the matrix often result in reduced water capture capacity. Therefore, on the basis of design principles, the entire preparation process should be coordinated from the perspectives of chemistry, materials, and engineering to maximize the water adsorption capacity and release efficiency at the same time.

In addition to this, the development of portable AWH devices is often overlooked by researchers. Portable AWH devices are expected to efficiently produce clean water from the atmosphere at rural areas or individual-scale emergent usage, with great potential to bring them closer to commercial viability. For instance, Wang's group developed a portable

https://doi.org/10.1021/acsmaterialsau.2c00027
ACS Mater. Au XXXX, XXX, XXX−XXX

device consisting of a PAM-$CaCl_2$ hydrogel as an AWH material and porous fabric omniphobic container.[13] Overall, improving the chemical and mechanical stability of AWH materials and developing suitable manufacturing techniques are important as the basis for designing recyclable, lightweight, and easy-to-install hydrogel-based commercial AWH equipment in the foreseeable future. Potential solutions, such as advanced manufacturing (e.g., 3D printing techniques),[28,122−124] have been applied to the fabrication of AWH materials but are far from widespread.

One knowledge gap in this field concerns the impact of air impurities (e.g., dust, bacteria, acidic gases, volatile organic compounds, etc) on the AWH process. In general, the adsorption of water molecules by AWH materials heavily relies on the hydrophilic functional groups and porous structure on the surface of the material. Dust, bacteria, and other particles in the air may adhere to the surface and block the pores, reducing water adsorption efficiency and capacity of the AWH materials during long-period operation. In addition, the acidic aqueous solution produced by the dissolution of acidic gases (SOx and NOx) would negatively affect the chemical structure of the AWH materials.[125,126] Furthermore, adsorbed volatile organic compounds (VOCs) are easily released together with captured water, thereby reducing the quality of produced water.[127,128] The solution of this challenge relies on the antibacterial ability of the material itself as well as the structural design and function customization of the water adsorption device. Air pollutants, particles, and microorganisms adsorbed on the surface of the AWH material or entering the interior are difficult to remove automatically because of their large size or insolubility in water. Therefore, interdisciplinary research team sincluding experts in chemical engineering, mechanical engineering, aerodynamics, and other fields are highly needed.

We have seen a preference for using low-cost chemicals and a desire to find a balance between cost and water-harvesting efficiency.[79,129] However, to date, there has been little available literature on the detailed cost analysis of water harvesting using passive AWH technologies. We call for an adequate assessment of the costs of materials, catchment devices, and support/maintenance to fill this research gap. For instance, the rating system should be based on a common unit, such as daily water production per dollar invested, pay-back period, and investigation-water production ratio per unit mass of material. In addition, current studies also overlooked the diffusion kinetics of H_2O from the surface to the interior. There is a huge difference in the diffusion process between different AWH materials, which is a very important aspect to understand AWH materials and provide design guidance for further AWH materials development.

5. CONCLUSIONS

In this Review, recent advances in materials chemistry for air−water harvesting applications have been critically discussed. Compared with traditional freshwater collection methods such as reverse osmosis in membrane seawater desalination, long-distance water delivery, and power-based active condensation devices, the new AWH materials do not need external mechanical equipment and external energy sources. The current high-efficiency AWH materials can produce about 6.5 kg of freshwater per day using 1 kg of hydrogel under optimal conditions, meeting the daily drinking water requirement of three adults, with no additional energy consumption. This makes these materials extremely competitive in the field of freshwater harvesting. Due to the broad prospects of AWH materials, it is expected that a technology based on them will play a major role in alleviating the shortage of freshwater resources in dry or water-deficient areas in the foreseeable future.

AUTHOR INFORMATION

Corresponding Author

Qiang Fu − *Centre for Technology in Water and Wastewater, School of Civil and Environmental Engineering, University of Technology Sydney, Ultimo, New South Wales 2007, Australia;* orcid.org/0000-0002-4012-330X; Email: Qiang.Fu@uts.edu.au

Authors

An Feng − *Centre for Technology in Water and Wastewater, School of Civil and Environmental Engineering, University of Technology Sydney, Ultimo, New South Wales 2007, Australia*

Nawshad Akther − *Centre for Technology in Water and Wastewater, School of Civil and Environmental Engineering, University of Technology Sydney, Ultimo, New South Wales 2007, Australia*

Xiaofei Duan − *Melbourne TrACEES Platform, School of Chemistry, The University of Melbourne, Melbourne, Victoria 3010, Australia*

Shuhua Peng − *School of Mechanical and Manufacturing Engineering, UNSW, Sydney, New South Wales 2052, Australia;* orcid.org/0000-0001-5680-9448

Casey Onggowarsito − *Centre for Technology in Water and Wastewater, School of Civil and Environmental Engineering, University of Technology Sydney, Ultimo, New South Wales 2007, Australia*

Shudi Mao − *Centre for Technology in Water and Wastewater, School of Civil and Environmental Engineering, University of Technology Sydney, Ultimo, New South Wales 2007, Australia*

Spas D. Kolev − *Melbourne TrACEES Platform, School of Chemistry and Department of Chemical Engineering, The University of Melbourne, Melbourne, Victoria 3010, Australia;* Present Address: Faculty of Chemistry and Pharmacy, Sofia University "St. Kl. Ohridski", 1 James Bourchier Blvd., 1164 Sofia, Bulgaria; orcid.org/0000-0003-4736-3039

Complete contact information is available at: https://pubs.acs.org/10.1021/acsmaterialsau.2c00027

Notes

The authors declare no competing financial interest.

ACKNOWLEDGMENTS

Q.F. acknowledges the Australian Research Council under the Future Fellowship (FT180100312). A.F. acknowledges support of the International Research Scholarship from the University of Technology Sydney.

REFERENCES

(1) Hanjra, M. A.; Qureshi, M. E. Global water crisis and future food security in an era of climate change. *Food policy* **2010**, *35* (5), 365−377.

https://doi.org/10.1021/acsmaterialsau.2c00027
ACS Mater. Au XXXX, XXX, XXX−XXX

(2) Gleick, P. H. *Water in crisis*; Oxford University Press: New York, 1993; Vol. *100*.
(3) Emery, W.; Meincke, J. Global water masses-summary and review. *Oceanol. Acta* **1986**, *9* (4), 383−391.
(4) Hinrichsen, D.; Tacio, H. The coming freshwater crisis is already here. *The linkages between population and water*; Woodrow Wilson International Center for Scholars: Washington, DC, 2002; pp 1−26.
(5) Schlosser, C. A.; Strzepek, K.; Gao, X.; Fant, C.; Blanc, É.; Paltsev, S.; Jacoby, H.; Reilly, J.; Gueneau, A. The future of global water stress: An integrated assessment. *Earth's Future* **2014**, *2* (8), 341−361.
(6) Zhu, X.; Zhang, C.; Yin, J.; Zhou, H.; Jiang, Y. Optimization of water diversion based on reservoir operating rules: Analysis of the Biliu River reservoir, China. *Journal of Hydrologic Engineering* **2014**, *19* (2), 411−421.
(7) Rodriguez, C. A.; Flessa, K. W.; Dettman, D. L. Effects of upstream diversion of Colorado River water on the estuarine bivalve mollusc Mulinia coloradoensis. *Conserv. Biol.* **2001**, *15* (1), 249−258.
(8) Briscoe, J. The changing face of water infrastructure financing in developing countries. *International Journal of Water Resources Development* **1999**, *15* (3), 301−308.
(9) Micale, G.; Rizzuti, L.; Cipollina, A. *Seawater desalination: conventional and renewable energy processes*; Springer: Berlin, Heidelberg, 2009; Vol. *1*.
(10) Karagiannis, I. C.; Soldatos, P. G. Water desalination cost literature: review and assessment. *Desalination* **2008**, *223* (1−3), 448−456.
(11) Wei, G.; Yang, Z.; Cui, B.; Li, B.; Chen, H.; Bai, J.; Dong, S. Impact of dam construction on water quality and water self-purification capacity of the Lancang River, China. *Water resources management* **2009**, *23* (9), 1763−1780.
(12) Al-Sahlawi, M. A. Seawater desalination in Saudi Arabia: economic review and demand projections. *Desalination* **1999**, *123* (2−3), 143−147.
(13) Li, R.; Wu, M.; Shi, Y.; Aleid, S.; Wang, W.; Zhang, C.; Wang, P. Hybrid water vapor sorbent design with pollution shielding properties: extracting clean water from polluted bulk water sources. *Journal of Materials Chemistry A* **2021**, *9* (26), 14731−14740.
(14) Hao, L.; Liu, N.; Bai, H.; He, P.; Niu, R.; Gong, J. High-performance solar-driven interfacial evaporation through molecular design of antibacterial, biomass-derived hydrogels. *J. Colloid Interface Sci.* **2022**, *608*, 840−852.
(15) Irshad, M. S.; Wang, X.; Abbasi, M. S.; Arshad, N.; Chen, Z.; Guo, Z.; Yu, L.; Qian, J.; You, J.; Mei, T. Semiconductive, Flexible MnO2 NWs/Chitosan Hydrogels for Efficient Solar Steam Generation. *ACS Sustainable Chem. Eng.* **2021**, *9* (10), 3887−3900.
(16) Pirouz, B.; Palermo, S. A.; Turco, M. Improving the Efficiency of Green Roofs Using Atmospheric Water Harvesting Systems (An Innovative Design). *Water* **2021**, *13* (4), 546.
(17) Caldas, L.; Andaloro, A.; Calafiore, G.; Munechika, K.; Cabrini, S. Water harvesting from fog using building envelopes: part I. *Water and environment journal: WEJ.* **2018**, *32* (4), 493−499.
(18) De Santo, A. V.; Alfani, A.; De Luca, P. Water vapour uptake from the atmosphere by some Tillandsia species. *Annals of Botany* **1976**, *40* (166), 391−394.
(19) Rijke, A. The water-holding mechanism of sandgrouse feathers. *Journal of Experimental Biology* **1972**, *56* (1), 195−200.
(20) Joubert, C.; Maclean, G. The structure of the water-holding feathers of the Namaqua sandgrouse. *African Zoology* **1973**, *8* (2), 141−152.
(21) Thickett, S. C.; Neto, C.; Harris, A. T. Biomimetic surface coatings for atmospheric water capture prepared by dewetting of polymer films. *Adv. Mater.* **2011**, *23* (32), 3718−3722.
(22) Chen, Z.; Zhang, Z. Recent progress in beetle-inspired superhydrophilic-superhydrophobic micropatterned water-collection materials. *Water Sci. Technol.* **2020**, *82* (2), 207−226.
(23) Ju, J.; Zheng, Y.; Jiang, L. Bioinspired one-dimensional materials for directional liquid transport. *Accounts of chemical research* **2014**, *47* (8), 2342−2352.
(24) Chen, D.; Li, J.; Zhao, J.; Guo, J.; Zhang, S.; Sherazi, T. A.; Li, S. Bioinspired superhydrophilic-hydrophobic integrated surface with conical pattern-shape for self-driven fog collection. *J. Colloid Interface Sci.* **2018**, *530*, 274−281.
(25) Comanns, P. Passive water collection with the integument: mechanisms and their biomimetic potential. *J. Exp. Biol.* **2018**, *221* (10), jeb153130.
(26) Li, J.; Guo, Z. Spontaneous directional transportations of water droplets on surfaces driven by gradient structures. *Nanoscale* **2018**, *10* (29), 13814−13831.
(27) Wang, X.; Zeng, J.; Yu, X.; Liang, C.; Zhang, Y. Water harvesting method via a hybrid superwettable coating with superhydrophobic and superhydrophilic nanoparticles. *Appl. Surf. Sci.* **2019**, *465*, 986−994.
(28) Zhu, P.; Chen, R.; Zhou, C.; Tian, Y.; Wang, L. Asymmetric fibers for efficient fog harvesting. *Chem. Eng. J.* **2021**, *415*, 128944.
(29) Uddin, M. N.; Desai, F. J.; Rahman, M. M.; Asmatulu, R. A highly efficient fog harvester of electrospun permanent superhydrophobic-hydrophilic polymer nanocomposite fiber mats. *Nanoscale advances* **2020**, *2* (1), 4627−4638.
(30) Moazzam, P.; Tavassoli, H.; Razmjou, A.; Warkiani, M. E.; Asadnia, M. Mist harvesting using bioinspired polydopamine coating and microfabrication technology. *Desalination* **2018**, *429*, 111−118.
(31) Shi, Y.; Ilic, O.; Atwater, H. A.; Greer, J. R. All-day fresh water harvesting by microstructured hydrogel membranes. *Nat. Commun.* **2021**, *12* (1), 2797.
(32) Gindl-Altmutter, W.; Keckes, J. The structure and mechanical properties of spines from the cactus Opuntia ficus-indica. *BioResources* **2012**, *7* (1), 1232−1237.
(33) Malainine, M. E.; Dufresne, A.; Dupeyre, D.; Mahrouz, M.; Vuong, R.; Vignon, M. R. Structure and morphology of cladodes and spines of Opuntia ficus-indica. Cellulose extraction and characterisation. *Carbohydr. Polym.* **2003**, *51* (1), 77−83.
(34) Vignon, M.; Heux, L.; Malainine, M.-E.; Mahrouz, M. Arabinan−cellulose composite in Opuntia ficus-indica prickly pear spines. *Carbohydr. Res.* **2004**, *339* (1), 123−131.
(35) Ju, J.; Xiao, K.; Yao, X.; Bai, H.; Jiang, L. Bioinspired conical copper wire with gradient wettability for continuous and efficient fog collection. *Adv. Mater.* **2013**, *25* (41), 5937−5942.
(36) Heng, X.; Xiang, M.; Lu, Z.; Luo, C. Branched ZnO wire structures for water collection inspired by cacti. *ACS Appl. Mater. Interfaces* **2014**, *6* (11), 8032−8041.
(37) Yi, S.; Wang, J.; Chen, Z.; Liu, B.; Ren, L.; Liang, L.; Jiang, L. Cactus-inspired conical spines with oriented microbarbs for efficient fog harvesting. *Advanced Materials Technologies* **2019**, *4* (12), 1900727.
(38) Peng, Y.; He, Y.; Yang, S.; Ben, S.; Cao, M.; Li, K.; Liu, K.; Jiang, L. Magnetically Induced Fog Harvesting via Flexible Conical Arrays. *Adv. Funct. Mater.* **2015**, *25* (37), 5967−5971.
(39) Cao, M.; Ju, J.; Li, K.; Dou, S.; Liu, K.; Jiang, L. Facile and Large-Scale Fabrication of a Cactus-Inspired Continuous Fog Collector. *Adv. Funct. Mater.* **2014**, *24* (21), 3235−3240.
(40) Zhou, H.; Zhang, M.; Li, C.; Gao, C.; Zheng, Y. Excellent Fog-Droplets Collector via Integrative Janus Membrane and Conical Spine with Micro/Nanostructures. *Small* **2018**, *14* (27), 1801335.
(41) Cheng, Y.; Zhang, S.; Liu, S.; Huang, J.; Zhang, Z.; Wang, X.; Yu, Z.; Li, S.; Chen, Z.; Zhao, Y.; Lai, Y.; Qian, X.; Xiao, C. Fog catcher brushes with environmental friendly slippery alumina microneedle structured surface for efficient fog-harvesting. *Journal of cleaner production* **2021**, *315*, 127862.
(42) Li, J.; Ran, R.; Wang, H.; Wang, Y.; Chen, Y.; Niu, S.; Arratia, P. E.; Yang, S. Aerodynamics-assisted, efficient and scalable kirigami fog collectors. *Nat. Commun.* **2021**, *12*, 5484.
(43) Feng, S.; Delannoy, J.; Malod, A.; Zheng, H.; Quéré, D.; Wang, Z. Tip-induced flipping of droplets on Janus pillars: From local reconfiguration to global transport. *Sci. Adv.* **2020**, *6* (28), eabb4540.
(44) Mohamed, M.; William, G.; Fatouh, M. Solar energy utilization in water production from humid air. *Sol. Energy* **2017**, *148*, 98−109.

https://doi.org/10.1021/acsmaterialsau.2c00027
ACS Mater. Au XXXX, XXX, XXX−XXX

(45) Jarimi, H.; Powell, R.; Riffat, S. Review of sustainable methods for atmospheric water harvesting. *International Journal of Low-Carbon Technologies* **2020**, *15* (2), 253−276.
(46) Chen, L.; Zhang, X.; Cheng, X.; Xie, Z.; Kuang, Q.; Zheng, L. The function of metal−organic frameworks in the application of MOF-based composites. *Nanoscale Advances* **2020**, *2* (7), 2628−2647.
(47) Li, H.; Eddaoudi, M.; O'Keeffe, M.; Yaghi, O. M. Design and synthesis of an exceptionally stable and highly porous metal-organic framework. *Nature* **1999**, *402* (6759), 276−279.
(48) Janiak, C. Functional Organic Analogues of Zeolites Based on Metal-Organic Coordination Frameworks. *Angewandte Chemie (International ed.)* **1997**, *36* (13−14), 1431−1434.
(49) Li, H.; Eddaoudi, M.; Groy, T. L.; Yaghi, O. M. Establishing Microporosity in Open Metal−Organic Frameworks: Gas Sorption Isotherms for Zn(BDC) (BDC = 1,4-Benzenedicarboxylate). *J. Am. Chem. Soc.* **1998**, *120* (33), 8571−8572.
(50) Abánades Lázaro, I.; Forgan, R. S. Application of zirconium MOFs in drug delivery and biomedicine. *Coord. Chem. Rev.* **2019**, *380*, 230−259.
(51) Qiao, C.; Zhang, R.; Wang, Y.; Jia, Q.; Wang, X.; Yang, Z.; Xue, T.; Ji, R.; Cui, X.; Wang, Z. Rabies Virus-Inspired Metal−Organic Frameworks (MOFs) for Targeted Imaging and Chemotherapy of Glioma. *Angewandte Chemie (International ed.)* **2020**, *59* (39), 16982−16988.
(52) Kobielska, P. A.; Howarth, A. J.; Farha, O. K.; Nayak, S. Metal−organic frameworks for heavy metal removal from water. *Coordination chemistry reviews* **2018**, *358* (C), 92−107.
(53) Qian, X.; Zhang, R.; Chen, L.; Lei, Y.; Xu, A. Surface Hydrophobic Treatment of Water-Sensitive DUT-4 Metal−Organic Framework To Enhance Water Stability for Hydrogen Storage. *ACS sustainable chemistry & engineering* **2019**, *7* (19), 16007−16012.
(54) Maes, M.; Schouteden, S.; Alaerts, L.; Depla, D.; De Vos, D. E. Extracting organic contaminants from water using the metal-organic framework CrIII(OH)·{O2C-C6H 4-CO2}. *Physical chemistry chemical physics: PCCP* **2011**, *13* (13), 5587−5589.
(55) Hasan, Z.; Jhung, S. H. Removal of hazardous organics from water using metal-organic frameworks (MOFs): Plausible mechanisms for selective adsorptions. *Journal of hazardous materials* **2015**, *283*, 329−339.
(56) Kim, H.; Yang, S.; Rao, S. R.; Narayanan, S.; Kapustin, E. A.; Furukawa, H.; Umans, A. S.; Yaghi, O. M.; Wang, E. N. Water harvesting from air with metal-organic frameworks powered by natural sunlight. *Science (American Association for the Advancement of Science)* **2017**, *356* (6336), 430−434.
(57) Hanikel, N.; Prévot, M. S.; Yaghi, O. M. MOF water harvesters. *Nature Nanotechnol.* **2020**, *15* (5), 348−355.
(58) Furukawa, H.; Gandara, F.; Zhang, Y.-B.; Jiang, J.; Queen, W. L.; Hudson, M. R.; Yaghi, O. M. Water adsorption in porous metal−organic frameworks and related materials. *J. Am. Chem. Soc.* **2014**, *136* (11), 4369−4381.
(59) Kim, D.; Liu, X.; Lah, M. S. Topology analysis of metal−organic frameworks based on metal−organic polyhedra as secondary or tertiary building units. *Inorganic Chemistry Frontiers* **2015**, *2* (4), 336−360.
(60) Wißmann, G.; Schaate, A.; Lilienthal, S.; Bremer, I.; Schneider, A. M.; Behrens, P. Modulated synthesis of Zr-fumarate MOF. *Microporous Mesoporous Mater.* **2012**, *152*, 64−70.
(61) Bon, V.; Senkovska, I.; Baburin, I. A.; Kaskel, S. Zr-and Hf-based metal−organic frameworks: tracking down the polymorphism. *Cryst. Growth Des.* **2013**, *13* (3), 1231−1237.
(62) Cunha, D.; Gaudin, C.; Colinet, I.; Horcajada, P.; Maurin, G.; Serre, C. Rationalization of the entrapping of bioactive molecules into a series of functionalized porous zirconium terephthalate MOFs. *J. Mater. Chem. B* **2013**, *1* (8), 1101−1108.
(63) Cavka, J. H.; Jakobsen, S.; Olsbye, U.; Guillou, N.; Lamberti, C.; Bordiga, S.; Lillerud, K. P. A new zirconium inorganic building brick forming metal organic frameworks with exceptional stability. *J. Am. Chem. Soc.* **2008**, *130* (42), 13850−13851.
(64) Schaate, A.; Roy, P.; Preuße, T.; Lohmeier, S. J.; Godt, A.; Behrens, P. Porous interpenetrated zirconium−organic frameworks (PIZOFs): a chemically versatile family of metal−organic frameworks. *Chem.−Eur. J.* **2011**, *17* (34), 9320−9325.
(65) Hu, Y.; Fang, Z.; Wan, X.; Ma, X.; Wang, S.; Fan, S.; Dong, M.; Ye, Z.; Peng, X. Carbon nanotubes decorated hollow metal−organic frameworks for efficient solar-driven atmospheric water harvesting. *Chem. Eng. J.* **2022**, *430*, 133086.
(66) Hu, Y.; Fang, Z.; Ma, X.; Wan, X.; Wang, S.; Fan, S.; Ye, Z.; Peng, X. CaCl2 Nanocrystals decorated photothermal Fe-ferrocene MOFs hollow microspheres for atmospheric water harvesting. *Applied materials today* **2021**, *23*, 101076.
(67) Troyano, J.; Carné-Sánchez, A.; Maspoch, D. Programmable self-assembling 3D architectures generated by patterning of swellable MOF-based composite films. *Adv. Mater.* **2019**, *31* (21), 1808235.
(68) Maher, H.; Rupam, T. H.; Rocky, K. A.; Bassiouny, R.; Saha, B. B. Silica gel-MIL 100 (Fe) Composite Adsorbents for Ultra-low Heat-Driven Atmospheric Water Harvester. *Energy* **2021**, 121741.
(69) Wu, Q.; Su, W.; Li, Q.; Tao, Y.; Li, H. Enabling Continuous and Improved Solar-Driven Atmospheric Water Harvesting with Ti3C2-Incorporated Metal−Organic Framework Monoliths. *ACS Appl. Mater. Interfaces* **2021**, *13* (32), 38906−38915.
(70) Tao, Y.; Li, Q.; Wu, Q.; Li, H. Embedding metal foam into metal−organic framework monoliths for triggering a highly efficient release of adsorbed atmospheric water by localized eddy current heating. *Materials Horizons* **2021**, *8* (5), 1439−1445.
(71) Karmakar, A.; Mileo, P. G.; Bok, I.; Peh, S. B.; Zhang, J.; Yuan, H.; Maurin, G.; Zhao, D. Thermo-Responsive MOF/Polymer Composites for Temperature-Mediated Water Capture and Release. *Angew. Chem., Int. Ed.* **2020**, *59* (27), 11003−11009.
(72) Gordeeva, L. G.; Tokarev, M. M.; Parmon, V. N.; Aristov, Y. I. Selective water sorbents for multiple application, 6. Freshwater production from the atmosphere. *Reaction kinetics and catalysis letters* **1998**, *65* (1), 153−159.
(73) Wang, J.; Dang, Y.; Meguerdichian, A. G.; Dissanayake, S.; Kankanam-Kapuge, T.; Bamonte, S.; Tobin, Z. M.; Achola, L. A.; Suib, S. L. Water Harvesting from the Atmosphere in Arid Areas with Manganese Dioxide. *Environmental science & technology letters* **2020**, *7* (1), 48−53.
(74) Zhou, X.; Lu, H.; Zhao, F.; Yu, G. Atmospheric water harvesting: a review of material and structural designs. *ACS Materials Letters* **2020**, *2* (7), 671−684.
(75) Wang, X.; Li, X.; Liu, G.; Li, J.; Hu, X.; Xu, N.; Zhao, W.; Zhu, B.; Zhu, J. An interfacial solar heating assisted liquid sorbent atmospheric water generator. *Angew. Chem.* **2019**, *131* (35), 12182−12186.
(76) Ejeian, M.; Entezari, A.; Wang, R. Solar powered atmospheric water harvesting with enhanced LiCl/MgSO4/ACF composite. *Applied Thermal Engineering* **2020**, *176*, 115396.
(77) Entezari, A.; Ejeian, M.; Wang, R. Super Atmospheric Water Harvesting Hydrogel with Alginate Chains Modified with Binary Salts. *ACS materials letters* **2020**, *2* (5), 471−477.
(78) Li, R.; Shi, Y.; Wu, M.; Hong, S.; Wang, P. Improving atmospheric water production yield: Enabling multiple water harvesting cycles with nano sorbent. *Nano energy* **2020**, *67*, 104255.
(79) Deng, F.; Wang, C.; Xiang, C.; Wang, R. Bioinspired topological design of super hygroscopic complex for cost-effective atmospheric water harvesting. *Nano energy* **2021**, *90*, 106642.
(80) Chen, Y.; Yu, Z.; Ye, Y.; Zhang, Y.; Li, G.; Jiang, F. Superelastic, Hygroscopic, and Ionic Conducting Cellulose Nanofibril Monoliths by 3D Printing. *ACS Nano* **2021**, *15* (1), 1869−1879.
(81) Deng, F.; Xiang, C.; Wang, C.; Wang, R. Sorption-tree with scalable hygroscopic adsorbent-leaves for water harvesting. *J. Mater. Chem. A* **2022**, *10*, 6576−6586.
(82) Yang, K.; Shi, Y.; Wu, M.; Wang, W.; Jin, Y.; Li, R.; Shahzad, M. W.; Ng, K. C.; Wang, P. Hollow spherical SiO2 micro-container encapsulation of LiCl for high-performance simultaneous heat reallocation and seawater desalination. *Journal of materials chemistry. A, Materials for energy and sustainability* **2020**, *8* (4), 1887−1895.

https://doi.org/10.1021/acsmaterialsau.2c00027
ACS Mater. Au XXXX, XXX, XXX−XXX

(83) Shan, H.; Pan, Q.; Xiang, C.; Poredoš, P.; Ma, Q.; Ye, Z.; Hou, G.; Wang, R. High-yield solar-driven atmospheric water harvesting with ultra-high salt content composites encapsulated in porous membrane. *Cell reports physical science* **2021**, *2* (12), 100664.
(84) Saravanan, G.; Heera, T. Ionic liquids: as a solvent for electrodeposition of metals and energy conversions. *Int. J. Renewable Energy Commer.* **2017**, *3* (2), 19−38.
(85) Maase, M.; Massonne, K. Biphasic acid scavenging utilizing ionic liquids: the first commercial process with ionic liquids. *In Ionic Liquids IIIB: Fundamentals, Progress, Challenges, and Opportunities*; Rogers, R. D., Seddon, K. R., Eds.; American Chemical Society, 2005.
(86) Zhang, S.; Zhang, Z. C. Novel properties of ionic liquids in selective sulfur removal from fuels at room temperature. *Green Chem.* **2002**, *4* (4), 376−379.
(87) Huang, W.; Zhu, W.; Li, H.; Shi, H.; Zhu, G.; Liu, H.; Chen, G. Heteropolyanion-based ionic liquid for deep desulfurization of fuels in ionic liquids. *Industrial & engineering chemistry research* **2010**, *49* (19), 8998−9003.
(88) Qi, H.; Wei, T.; Zhao, W.; Zhu, B.; Liu, G.; Wang, P.; Lin, Z.; Wang, X.; Li, X.; Zhang, X. An interfacial solar-driven atmospheric water generator based on a liquid sorbent with simultaneous adsorption−desorption. *Adv. Mater.* **2019**, *31* (43), 1903378.
(89) Zhang, W.; Xia, Y.; Wen, Z.; Han, W.; Wang, S.; Cao, Y.; He, R.-X.; Liu, Y.; Chen, B. Enhanced adsorption-based atmospheric water harvesting using a photothermal cotton rod for freshwater production in cold climates. *RSC Adv.* **2021**, *11* (56), 35695−3572.
(90) Carrete, J.; García, M.; Rodríguez, J. R.; Cabeza, O.; Varela, L. M. Theoretical model for moisture adsorption on ionic liquids: A modified Brunauer−Emmet−Teller isotherm approach. *Fluid phase equilibria* **2011**, *301* (1), 118−122.
(91) Xu, J.; Liu, X.; Ren, X.; Gao, G. The role of chemical and physical crosslinking in different deformation stages of hybrid hydrogels. *Eur. Polym. J.* **2018**, *100*, 86−95.
(92) Gyles, D. A.; Castro, L. D.; Silva, J. O. C., Jr; Ribeiro-Costa, R. M. A review of the designs and prominent biomedical advances of natural and synthetic hydrogel formulations. *Eur. Polym. J.* **2017**, *88*, 373−392.
(93) Guo, Y.; Bae, J.; Fang, Z.; Li, P.; Zhao, F.; Yu, G. Hydrogels and hydrogel-derived materials for energy and water sustainability. *Chem. Rev.* **2020**, *120* (15), 7642−7707.
(94) Wang, W.; Tang, B.; Ju, B.; Gao, Z.; Xiu, J.; Zhang, S. Fe 3 O 4-functionalized graphene nanosheet embedded phase change material composites: efficient magnetic-and sunlight-driven energy conversion and storage. *Journal of Materials Chemistry A* **2017**, *5* (3), 958−968.
(95) Tang, B.; Qiu, M.; Zhang, S. Thermal conductivity enhancement of PEG/SiO2 composite PCM by in situ Cu doping. *Sol. Energy Mater. Sol. Cells* **2012**, *105*, 242−248.
(96) Yang, Y.; Yang, X.; Fu, L.; Zou, M.; Cao, A.; Du, Y.; Yuan, Q.; Yan, C.-H. Two-dimensional flexible bilayer janus membrane for advanced photothermal water desalination. *ACS Energy Letters* **2018**, *3* (5), 1165−1171.
(97) Entezari, A.; Ejeian, M.; Wang, R. Super atmospheric water harvesting. hydrogel with alginate chains modified with binary salts. *ACS Materials Letters* **2020**, *2* (5), 471−477.
(98) Ni, F.; Qiu, N.; Xiao, P.; Zhang, C.; Jian, Y.; Liang, Y.; Xie, W.; Yan, L.; Chen, T. Tillandsia-Inspired Hygroscopic Photothermal Organogels for Efficient Atmospheric Water Harvesting. *Angew. Chem., Int. Ed.* **2020**, *59* (43), 19237−19246.
(99) Kallenberger, P. A.; Fröba, M. Water harvesting from air with a hygroscopic salt in a hydrogel−derived matrix. *Commun. Chem.* **2018**, *1* (1), 28.
(100) Chen, B.; Zhao, X.; Yang, Y. Superelastic graphene nanocomposite for high cycle-stability water capture−release under sunlight. *ACS Appl. Mater. Interfaces* **2019**, *11* (17), 15616−15622.
(101) Kabir, A.; Dunlop, M. J.; Acharya, B.; Bissessur, R.; Ahmed, M. Water recycling efficacies of extremely hygroscopic, antifouling hydrogels. *RSC Adv.* **2018**, *8* (66), 38100−38107.
(102) Wu, M.; Li, R.; Shi, Y.; Altunkaya, M.; Aleid, S.; Zhang, C.; Wang, W.; Wang, P. Metal-and halide-free, solid-state polymeric water vapor sorbents for efficient water-sorption-driven cooling and atmospheric water harvesting. *Materials Horizons* **2021**, *8* (5), 1518−1527.
(103) Li, R.; Shi, Y.; Alsaedi, M.; Wu, M.; Shi, L.; Wang, P. Hybrid hydrogel. with high water vapor harvesting capacity for deployable solar-driven atmospheric water generator. *Environ. Sci. Technol.* **2018**, *52* (19), 11367−11377.
(104) Xu, J.; Li, T.; Yan, T.; Wu, S.; Wu, M.; Chao, J.; Huo, X.; Wang, P.; Wang, R. Ultrahigh solar-driven atmospheric water production enabled by scalable rapid-cycling water harvester with vertically aligned nanocomposite sorbent. *Energy Environ. Sci.* **2021**, *14* (11), 5979−5994.
(105) Lei, C.; Guo, Y.; Guan, W.; Lu, H.; Shi, W.; Yu, G. Polyzwitterionic Hydrogels for Efficient Atmospheric Water Harvesting. *Angew. Chem. Int. Ed.* **2022**, e202200271.
(106) Aleid, S.; Wu, M.; Li, R.; Wang, W.; Zhang, C.; Zhang, L.; Wang, P. Salting-in Effect of Zwitterionic Polymer Hydrogel Facilitates Atmospheric Water Harvesting. *ACS Materials Letters* **2022**, *4* (3), 511−520.
(107) Jin, S.; Liu, M.; Chen, S.; Gao, C. Synthesis, characterization and the rapid response property of the temperature responsive PVP-g-PNIPAM hydrogel. *European polymer journal* **2008**, *44* (7), 2162−2170.
(108) Zhang, H.; Niu, Q.; Wang, N.; Nie, J.; Ma, G. Thermo-sensitive drug controlled release PLA core/PNIPAM shell fibers fabricated using a combination of electrospinning and UV photo-polymerization. *Eur. Polym. J.* **2015**, *71*, 440−450.
(109) Pelton, R. Poly (N-isopropylacrylamide)(PNIPAM) is never hydrophobic. *J. Colloid Interface Sci.* **2010**, *348* (2), 673−674.
(110) Larson, J. W.; McMahon, T. B. Gas-phase bihalide and pseudobihalide. ions. An ion cyclotron resonance determination of hydrogen bond energies in XHY-species (X, Y= F, Cl, Br, CN). *Inorg. Chem.* **1984**, *23* (14), 2029−2033.
(111) Benson, S. W. III-Bond energies. *J. Chem. Educ.* **1965**, *42* (9), 502.
(112) Zhao, F.; Zhou, X.; Liu, Y.; Shi, Y.; Dai, Y.; Yu, G. Super moisture-absorbent gels for all-weather atmospheric water harvesting. *Adv. Mater.* **2019**, *31* (10), 1806446.
(113) Cadiau, A.; Lee, J. S.; Damasceno Borges, D.; Fabry, P.; Devic, T.; Wharmby, M. T.; Martineau, C.; Foucher, D.; Taulelle, F.; Jun, C.-H.; Hwang, Y. K.; Stock, N.; De Lange, M. F.; Kapteijn, F.; Gascon, J.; Maurin, G.; Chang, J.-S.; Serre, C. Design of Hydrophilic Metal Organic Framework Water Adsorbents for Heat Reallocation. *Advanced materials (Weinheim)* **2015**, *27* (32), 4775−4780.
(114) Rieth, A. J.; Wright, A. M.; Skorupskii, G.; Mancuso, J. L.; Hendon, C. H.; Dincă, M. Record-Setting Sorbents for Reversible Water Uptake by Systematic Anion Exchanges in Metal−Organic Frameworks. *J. Am. Chem. Soc.* **2019**, *141* (35), 13858−13866.
(115) Fathieh, F.; Kalmutzki, M. J.; Kapustin, E. A.; Waller, P. J.; Yang, J.; Yaghi, O. M. Practical water production from desert air. *Science advances* **2018**, *4* (6), eaat3198.
(116) Towsif Abtab, S. M.; Alezi, D.; Bhatt, P. M.; Shkurenko, A.; Belmabkhout, Y.; Aggarwal, H.; Weseliński, Ł. J.; Alsadun, N.; Samin, U.; Hedhili, M. N.; Eddaoudi, M. Reticular Chemistry in Action: A Hydrolytically Stable MOF Capturing Twice Its Weight in Adsorbed Water. *Chem.* **2018**, *4* (1), 94−105.
(117) Liu, X.; Wang, W.; Xie, S.; Pan, Q. Performance characterization and application of composite adsorbent LiCl@ ACFF for moisture harvesting. *Sci. Rep.* **2021**, *11* (1), 14412.
(118) Li, C.; Zhu, J.; Zhou, M.; Zhang, S.; He, X. Investigation on Water Vapor Adsorption of Silica-Phosphonium Ionic Liquids Hybrid Material. *Materials* **2019**, *12* (11), 1782.
(119) Nandakumar, D. K.; Zhang, Y.; Ravi, S. K.; Guo, N.; Zhang, C.; Tan, S. C. Solar energy triggered clean water harvesting from humid air existing above sea surface enabled by a hydrogel with ultrahigh hygroscopicity. *Adv. Mater.* **2019**, *31* (10), 1806730.
(120) Yilmaz, G.; Meng, F. L.; Lu, W.; Abed, J.; Peh, C. K. N.; Gao, M.; Ho, G. W, Autonomous atmospheric water seeping MOF matrix. *Sci. Adv.* **2020**, *6* (42), eabc8605.

https://doi.org/10.1021/acsmaterialsau.2c00027
ACS Mater. Au XXXX, XXX, XXX−XXX

(121) Lord, J.; Thomas, A.; Treat, N.; Forkin, M.; Bain, R.; Dulac, P.; Behroozi, C. H.; Mamutov, T.; Fongheiser, J.; Kobilansky, N.; et al. Global potential for harvesting drinking water from air using solar energy. *Nature* **2021**, *598* (7882), 611−617.
(122) Huang, B.; Zhou, Z.; Wei, L.; Song, Q.; Yu, W.; Zhou, Y.; Hu, R.; Zhang, W.; Lu, C. Ti3C2Tx MXene as a novel functional photo blocker for stereolithographic 3D printing of multifunctional gels via Continuous Liquid Interface Production. *Composites. Part B, Engineering* **2021**, *225*, 109261.
(123) Ciffreo, L.; Marchand, C.; Szczepanski, C. R.; Medici, M.-G.; Godeau, G. Bioinspired and Post-Functionalized 3D-Printed Surfaces with Parahydrophobic Properties. *Biomimetics (Basel, Switzerland)* **2021**, *6* (4), 71.
(124) Lu, H.; Shi, W.; Guo, Y.; Guan, W.; Lei, C.; Yu, G. Materials Engineering for Atmospheric Water Harvesting: Progress and Perspectives. *Adv. Mater* **2022**, *34* (12), 2110079.
(125) Betancourt, T.; Pardo, J.; Soo, K.; Peppas, N. A. Characterization of pH-responsive hydrogels of poly(itaconic acid-g-ethylene glycol) prepared by UV-initiated free radical polymerization as biomaterials for oral delivery of bioactive agents. *J. Biomed. Mater. Res., Part A* **2010**, *93A* (1), 175−188.
(126) Tuan Mohamood, N. F. A.-Z.; Zainuddin, N.; Ahmad@Ayob, M.; Tan, S. W. Preparation, optimization and swelling study of carboxymethyl sago starch (CMSS)−acid hydrogel. *Chem. Cent. J.* **2018**, *12* (1), 133.
(127) Li, H.; Guo, J.; Ren, J.; Li, Y.; Yu, X. Carbon nanodot-induced Eu-based fluorescent polymeric hydrogel for excellent phase-separation absorption of VOC. *J. Mater. Chem. A* **2022**, *10* (14), 7941−7947.
(128) Parafati, L.; Vitale, A.; Restuccia, C.; Cirvilleri, G. Performance evaluation of volatile organic compounds by antagonistic yeasts immobilized on hydrogel spheres against gray, green and blue postharvest decays. *Food microbiology* **2017**, *63*, 191−198.
(129) Gado, M. G.; Nasser, M.; Hassan, A. A.; Hassan, H. Adsorption-based atmospheric water harvesting powered by solar energy: Comprehensive review on desiccant materials and systems. *Process safety and environmental protection* **2022**, *160*, 166−183.

https://doi.org/10.1021/acsmaterialsau.2c00027
ACS Mater. Au XXXX, XXX, XXX−XXX